Journal of Comparative Neurology

WILEY

JCN RESEARCH IN SYSTEMS NEUROSCIENCE THE JOURNAL OF COMPARATIVE NEUROLOGY

RESEARCH ARTICLE OPEN ACCESS

Vascular Development of Fetal and Postnatal Neocortex of the Pig, the European Wild Boar *Sus scrofa*

Eric Sobierajski[1] | Katrin Czubay[1] | Christa Beemelmans[2] | Christoph Beemelmans[2] | Martin Meschkat[3] | Dennis Uhlenkamp[3] | Gundela Meyer[4] | Petra Wahle[1]

[1]Department of Developmental Neurobiology, Faculty of Biology and Biotechnology, Ruhr University Bochum, Bochum, Germany | [2]Regionalverband Ruhr Grün, Forsthof Üfter Mark, Schermbeck, Germany | [3]Abberior Instruments GmbH, Göttingen, Germany | [4]Department of Basic Medical Science, Faculty of Medicine, University of La Laguna, Santa Cruz de Tenerife, Tenerife, Spain

Correspondence: Petra Wahle (petra.wahle@rub.de)

Received: 23 May 2024 | **Revised:** 14 October 2024 | **Accepted:** 21 October 2024

Funding: This work was supported by Deutsche Forschungsgemeinschaft WA 541/15-1 to P. W.

Keywords: pericytic cells | microglia cells | GABAergic neurons | ungulate | porcine

ABSTRACT

The development of the brain's vascular system is a predominantly prenatal process in mammalian species and is required for neurogenesis and further brain development. Our recent work on fetal pig has revealed that many neurodevelopmental processes start well before birth and proceed rapidly reaching near-mature status already around birth. Here, we analyzed the development of neocortical vasculature from embryonic day (E) 45 onward (gestation in pig lasts 114 days) using qualitative and quantitative image analyses and protein blots. In all cortical layers, vessel volume from total brain volume at E100 resembled that of a postnatal day (P) 30 piglet. Endothelial cells expressed the tight junction protein claudin-5 from E45 onward. GFAP+ and AQP4+ astrocytes, PDGFRβ+ pericytes, and α-SMA+ smooth muscle cells are detectable near vessels at E60 suggesting an early assembly of blood–brain barrier components. The vascular system in the visual cortex is advanced before birth with an almost mature pattern at E100. Findings were confirmed by blots that showed a steady increase of expression of tight junction and angiogenesis-related proteins (claudin-5, occludin, VE-cadherin, PECAM-1/CD31) from E65 onward until P90. The expression profile was similar in visual and somatosensory cortex. Together, we report a rapid maturation of the vascular system in pig cortex.

1 | Introduction

Most of the research on cortical development to date is still done with small rodents besides nonhuman primates and human. The pig as an alternative experimental and translational model is a precocial nest fledgling with almost fully formed sensory and motor systems at birth. The pig brain resembles the human brain with respect to its high cortical gyration index and neuron count (Zilles, Palomero-Gallagher, and Amunts 2013). A recent genome exploration of the pig (Teng et al. 2024) also demonstrates the high similarity of gene expression in various body organs between pig and human.

The vascular system delivers oxygen as well as hormones, glucose, and metabolites, serves the tissue homeostasis and as waste disposal (Andreone, Lacoste, and Gu 2015). The vascular network is adapted to the local metabolic demand (Ji et al. 2021). Delivery of immune cells seeding the diploë of the skull and the meninges installs a line of defense, which can rapidly contribute to protection against pathogens and infection. Interactions between endothelial cells and the neuronal environment are necessary for the formation of the blood–brain barrier (BBB) (Stewart and Wiley 1981), which separates vasculature and the central nervous system (CNS). The cellular elements contributing to the BBB are summarized under the term neurovascular unit. Well

characterized are the roles of astrocytes and microglia (Thurgur and Pinteaux 2019). Furthermore, pericytes participate in the control of blood flow (Armulik et al. 2010; Attwell et al. 2016; Grubb et al. 2020; Hall et al. 2014). Both, astrocytes and capillary pericytes were observed to be innervated by local neurons for neurovascular coupling (Andreone, Lacoste, and Gu 2015; Kisler et al. 2017b). A permanent crosstalk between the contributing cell types ensures the functional integrity of the BBB in the healthy brain, or the recovery after a pathological insult (Kozma et al. 2021; Liu et al. 2020).

Recently, neurovascular unit disruption has been studied in newborn pig with fetal growth restriction. Treatment with the anti-inflammatory drug ibuprofen attenuates BBB disruption, reduces overall proinflammatory responses, and promotes tighter vasculature-astrocytic end feet contacts, which restores neurovascular unit integrity (Chand et al. 2022). In the case of neurological diseases such as Alzheimer's disease (Clark et al. 2022; Kisler et al. 2017a), multiple sclerosis (Kaushik et al. 2021), or schizophrenia (Greene et al. 2017), the crosstalk can be impaired. This can lead to an altered BBB permeability enabling the infiltration of toxins, proinflammatory molecules, and cells into the brain (Cayrol et al. 2008; Haruwaka et al. 2019). Developmentally, the absence of pericytes during embryogenesis leads to damaged integrity and leaky BBB (Daneman et al. 2010; Mäe et al. 2021). A number of recent discoveries have extended our knowledge. A fourth meningeal layer, the subarachnoid lymphatic-like membrane has been characterized (Møllgård et al. 2023) with the hypothetical function of a filter membrane. Additionally, evidence emerged that the dura mater is directly connected to the brain via bridging veins that form structures termed arachnoid cuffs (Smyth et al. 2024). Moreover, vascular endothelial cells collected from different brain regions display a surprising variability in gene expression, which might even influence progression rates of Alzheimer's disease (Bryant et al. 2023).

The vascular system develops in synchrony with the brain (Segarra et al. 2019). In the chicken embryo, the neural tube is already encircled by a vascular plexus, which subsequently extends endothelial sprouts penetrating into the neural tissue (Feeney and Watterson 1946). Cajal-Retzius neurons (Meyer 2010) promote endothelial cell proliferation and angiogenesis (the creation of new vessels from preexisting ones), which stimulates radial glia cell attachment to the gliovascular basal lamina to ensure proper cortical neuron migration (Biswas, Cottarelli, and Agalliu 2020). Radial glia cells also anchor to local blood vessels and disruption of these interactions impairs the immigration of interneurons (Tan et al. 2016). Depleting vascular reelin signaling alters neocortical vascularization and disrupts the assembly of radial glial cell contacts at the pial surface. Thus, abrogation of vascular reelin signaling partially recapitulates the neural defects observed in the absence of reelin protein (Thomas 2018). Later on, neuronal activity influences vascular refinement as has been shown for the laminar-specific angiogenesis in visual cortex (VC) of marmoset (Fonta and Imbert 2002).

In previous studies of fetal pig cortex, we describe the rapid development of the Neuropeptide Y neuron system (Ernst et al. 2018; Sobierajski et al. 2022) and of microglia in the cortical laminar compartments (Sobierajski et al. 2022). Also, myelination begins early with the first oligodendrocyte progenitors found at E45 and large amounts of myelinated axons being present already at E100. Expression of myelin-related proteins commences 1–2 weeks earlier in the somatosensory compared with the VC which suggests a driving role of specific somatosensory activity (Sobierajski et al. 2023). The present study analyzes vascular development in VC and the expression of selected proteins in visual and somatosensory cortex (SC).

2 | Material and Methods

2.1 | Animal Material

The material for the immunohistochemical staining is from our fetal pig brain collection (Ernst et al. 2018; Sobierajski et al. 2023). Our model of choice is a nondomesticated form, the European wild boar, *Sus scrofa* (Linné 1758; Ritter et al. 2023). One argument for the wild representative comes from the fact that domestication of pig has resulted in a substantial reduction of brain weight by about 41% in comparison with wild boar (Böndel 2017), and brain endocast volume by about 18% (Cucchi et al. 2024). The second reason is that the material was obtained at no extra costs from the Üfter Mark area managed by the Regionalverband Ruhr Grün. Fetuses derived from mostly young (first pregnancy) sows and piglets individually hunted for population control in accordance with the German Game Law (Jagdrecht) or killed in road accidents. Law requests disposal of viscera including sexual organs. During evisceration at the Forsthof Üfter Mark, the uteri were examined for pregnancies. Embryonic membranes were removed, and fetuses immersed in cold 4% paraformaldehyde (PFA) in 0.1 M phosphate buffer pH 7.4. The P5 domestic "German Landrace" piglet was donated by the Institutes of Physiology and Anatomy, Medical Faculty, University Mannheim (donated by Prof. Martin Schmelz and Prof. Dr Maren Engelhardt). Staging has been done using the crown-rump-length formula (Henry 1968) for European wild boar and by external features. The term "gestational age" indicates the proportional fetal age with birth in pig at E114 and birth in sheep at E145 set to 1; it has been calculated to align fetal stages in pig and sheep. Fine dissection of the brain and the body organs was done after transport to Ruhr University. The meninges were largely removed to minimize cryostat cutting artifacts.

2.2 | Tissue Processing and Immunostaining Procedures

All litters prepared for immunohistochemistry and for protein blots, respectively, have been listed in detail earlier (see Table 1 in Sobierajski et al. 2023). Dissected brains were immersion-fixed in 4% PFA in 0.1 M phosphate buffer pH 7.4 with 5% (vol/vol) water-saturated picric acid for about 2 weeks at 8°C (refreshed once). After cryoprotection, tissue slabs were stored frozen in TissueTek (Sakura Finetek, Alphen aan den Rijn, Netherlands) at −80°C until cutting. Coronal 25 µm cryostat sections of occipital cortex mounted on silanized slides were submitted to antigen retrieval (40 min citrate buffer pH 5–6 at 80°C and cooling down slowly for about 1 h) followed by immunohistochemistry as previously described (Sobierajski et al. 2022). Blood vessels have been stained with tomato lectin, isolectin B4 (IB4), or PECAM1. Tomato lectin is a superior marker for blood vessels in normal

TABLE 1 | Antibodies and reagents for immunohistochemical staining and protein blotting.

Primary antibodies	Species, label, method	Source, order number, RRID	Dilution
Alpha-smooth muscle actin	Rabbit, IF, WB	Abcam, Cambridge, UK, Cat# ab5694, RRID: AB_2223021	1:200 (IF) 1:1000 (WB)
Aquaporin 4	Guinea pig, IF, WB	Synaptic Systems, Göttingen, DE, Cat# 429004, RRID: AB_2802156	1:800 (IF) 1:1000 (WB)
Claudin-5	Mouse, IF, WB	ThermoFisher Scientific, Darmstadt, DE, Cat# 35-2500, RRID: AB_2533200	1:200 (IF)
Glial fibrillary acidic protein	Rabbit, IF	Dako A/S, Glostrup, DEN, Cat# Z0334, RRID: AB_10013382	1:400 (IF)
Isolectin B4 (*Bandeiraea simplicifolia*)	FITC, IF	Enzo Life Sciences GmbH, Lörrach, DE, Cat# ALX-650-001F	1:400 (IF)
Occludin	Guinea pig, WB	Synaptic Systems, Göttingen, DE, Cat# 447005, RRID: AB_2884909	1:1000 (WB)
Platelet-derived growth factor receptor beta	Goat, IF, WB	R&D Systems, Minneapolis, MN, USA, Cat# AF385, RRID: AB_355339	1:500 (IF) 1:1000 (WB)
Platelet endothelial cell adhesion molecule 1	Guinea pig, IF, WB	Synaptic Systems, Göttingen, DE Cat# HS351004, RRID: AB_2620105	1:300 (IF)
Platelet endothelial cell adhesion molecule 1	Mouse, IF, WB	Santa Cruz Biotechnology, Dallas, Texas, USA, Cat# sc-376764, RRID: AB_2801330	1:1000 (WB)
Vascular endothelial cadherin	Goat, WB	Santa Cruz Biotechnology, Dallas, Texas, USA, Cat# sc-6458, RRID: AB_2077955	1:1000 (WB)
β-actin (housekeeping protein)	Mouse, WB	Sigma–Aldrich, St. Louis, MO, USA, Cat# A1978, RRID: AB_476692	1:6000 (WB)
β-Tubulin (housekeeping protein)	Mouse, WB	Sigma–Aldrich, St. Louis, MO, USA, Cat# T8660, RRID: AB_477590	1:3000 (WB)
Tomato lectin (*Lycopersicon esculentum*)	biotin, IF, IHC	Sigma–Aldrich, St. Louis, MO, USA, Cat# L0651	1:500 (IF, IHC)
Secondary antibodies			
Streptavidin	DyLight 594, IF	ThermoFisher Scientific, Darmstadt, DE, Cat# 21842 RRID: AB_2619631	1:1000 (IF)
Anti-rabbit	Donkey, Alexa-488, IF	Thermo Scientific, Waltham MA, USA, RRID: AB_2687506	1:1000 (IF)
Anti-mouse	Goat, Alexa-568, IF	Invitrogen, Carlsbad, CA, USA, RRID: AB_2534013	1:1000 (IF)
Anti-guinea pig	Goat, Alexa-488, IF	Thermofisher Scientific, Darmstadt, DE, Cat# A11073, RRID: AB_2534117	1:1000 (IF)
Anti-guinea pig	Donkey, Alexa-594, IF	Dianova, Cat# 706-757-148	1:1000 (IF)
Anti-guinea pig	Goat, Star Green, IF	Abberior dyes, Göttingen, DE, Cat# STGREEN-1006-500UG	1:200 (IF)
Anti-rabbit or anti-mouse	Goat, Star Red, IF	Abberior dyes, Göttingen, DE, Cat# STRED-1002-500UG	1:200 (IF)
Anti-rabbit or anti-mouse	Goat, Star Orange, IF	Abberior dyes, Göttingen, DE, Cat# STORANGE-1001-500UG	1:200 (IF)
Anti-mouse	Rabbit, alkaline phosphatase, WB	Dako A/S, Glostrup, DEN, Cat# D0314	1:5000 (WB)

(Continues)

TABLE 1 | (Continued)

Primary antibodies	Species, label, method	Source, order number, RRID	Dilution
Anti-goat	Donkey, alkaline phosphatase, WB	Life Technologies, Carlsbad, CA, USA, Cat# A16002, RRID: AB_2534676	1:2000 (WB)
Anti-rabbit	Goat, alkaline phosphatase, WB	Dako, Hamburg, DE, Cat# D0487, RRID: AB_2617144	1:3000 (WB)
Anti-guinea pig	Goat, alkaline phosphatase, WB	ThermoFisher Scientific, Darmstadt, DE, Cat# A18772	1:5000 (WB)
Reagents			
Tetrahydrofuran	Lipid removal	Sigma–Aldrich St. Louis, MO, USA, Cat# 186562	50% (v/v)
Nycodenz	Transparent rendering	Serumwerk Bernburg AG, Bernburg, DE, Cat# 18003	80% (w/v)
DAPI	Fluorescent counterstain	Sigma–Aldrich, St. Louis, MO, USA, Cat# D9542	1:2500
Sudan Black	To quench autofluorescence	Merck, Darmstadt, DE, Cat# 1387	0.2% (w/v)
ABC reagent	Horseradish peroxidase;	Vector Laboratories, Inc., Burlingame, CA, USA, Cat# PK-6100, RRID: AB_2336827	6 µL vector A/B per mL TBS
Diaminobenzidine DAB	Chromogen	Sigma–Aldrich, Steinheim, DE, Cat# D12384	0.02% (v/v)
Osmium tetroxide	Intensification	Sigma–Aldrich, Steinheim, DE, Cat# O5500	1%

Abbreviations: IHC, immunohistochemistry with DAB staining; IF, immunofluorescence; WB, Western blot.

tissue (Battistella et al. 2021). IB4 marks vessels (Battistella et al. 2021; Gama Sosa et al. 2021). It also marks macrophages and activated microglia by binding to the Ret receptor (Boscia et al. 2013). IB4 labeling intensity decreases from fetal to postnatal in rodent (Wu et al. 1994). Antibodies and lectins are listed in Table 1. Immunofluorescent labeling was combined with a quenching of autofluorescence by incubation in Sudan Black B (0.2%, w/v, dissolved in 70% isopropyl alcohol) for about 60 min before incubation of the secondary antibody. A brief incubation with DAPI was done before coverslipping to delineate cortical layers and mark cell nuclei. Alternatively, we used biotinylated secondaries followed by avidin–biotin–horseradish peroxidase complex and 3,3-diaminobenzidine. The DAB reaction product was intensified with 1% OsO_4 in phosphate buffer for 1–2 min. Finally, the sections were dehydrated and coverslipped with DPX (Sigma–Aldrich, Steinheim, Germany). In some cases, a counterstain with thionin was done before dehydration. No specific staining remained after omitting the primary and/or secondary antibodies except for autofluorescence of blood cells.

2.3 | Tissue Clearing

Vibratome sections with a thickness of 300 µm were treated with the "EZ Clear" method (Hsu et al. 2022). In brief, the slices were washed in tetrahydrofuran for 16 h in light-protected glass scintillation vials, then washed four times for 1 h each in distilled water. After washing, immunofluorescent labeling was performed with the blocking step increased to 1 day and the incubation times of the primary and secondary antibody each increased to 2 days at room temperature. Thereafter, sections were incubated for 1 day in EZ clear solution (7 M urea, 0.05% N-azide, 80% Nycodenz in 0.02 M phosphate buffer pH 7.4) until they rendered transparent. For confocal images, the slices were embedded with EZ view solution in μ-dishes (ibidi GmbH, Gräfeling, Germany) and flattened with a piece of foil to obtain a planar focus level.

2.4 | Western Blots

As described (Sobierajski et al. 2023), tissue blocks of visual and SC were taken during preparation of the fetuses (ages E65, E80, E95, E100, and P90) and frozen on dry ice for storage. Small blocks were first pulverized on dry ice. Microspoon-sized samples of the powder were homogenized in standard RIPA buffer. Protein amount was determined with the Markwell protein assay. For SDS-PAGE, proteins were separated on 10 or 14% polyacrylamide gels (30 mg per lane) with a current voltage of 7 mA per gel overnight. Proteins were transferred to nitrocellulose membranes (BA 85; Schleicher and Schuell, Germany) with a tank blotter (Hoefer, San Francisco, CA, USA). Smaller proteins were transferred with buffer containing 20% MeOH, proteins above 100 kDa were transferred with buffer containing 15% MeOH and 0.05% SDS. Membranes were cut into horizontal stripes (Engelhardt et al. 2018) containing the desired protein bands such

that up to eight proteins of different molecular weights could be concurrently detected in each lysate. Membranes were blocked with TBS (50 mM Tris–HCl, pH 7.4, 150 mM NaCl) containing 5% bovine serum albumin for 2 h. Primary antibodies (Table 1) were incubated overnight at 4°C, followed by washes for 10 min in TBST (50 mM Tris, pH 7.4, 150 mM NaCl, 0.1% Tween-20) and 10 min in TBS. Appropriate alkaline phosphatase-conjugated secondaries were incubated for 90 min. Blots were stained with 0.18 mg/mL BCIP and 0.35 mg/mL NBT in an alkaline buffer (100 mM Tris–HCl, pH 9.5, 50 mM $MgCl_2$), rinsed with water and dried.

2.5 | Analysis

DAB-stained material was analyzed with light microscopy. The E45 plot was done from thionin-stained sections with the Neurolucida (MicroBrightField, Inc., Williston, Vermont, USA). Bright field photomicrographs were taken with a Zeiss Axiophot equipped with a CCD camera (PCO, Kelheim, Germany). Images and plots were arranged with Adobe Photoshop (CS6 Extended, Version 13.0×64) and Inkscape (open-source software). Regions of interest were selected with the aim to document the distribution of pericytes or vasculature in the laminar compartments at selected fetal and postnatal stages. Fluorescent images and tile scans were done with a Leica TSC SP5 confocal microscope (10× and 40× objective with 1.1 NA, 1024 × 1024 px). Global whole-picture contrast, brightness, color intensity, and saturation settings were adjusted with Adobe Photoshop. Scale bars were generated with ImageJ (MacBiophotonics) and inserted with Adobe Photoshop.

STED imaging was performed on a commercial STED microscope (Facility Line, Abberior Instruments, Germany) working at a repetition rate of 40 Mhz. Samples were immunostained using a FITC-coupled lectin or antibodies with appropriate secondaries conjugated to the dyes STAR RED, STAR ORANGE, and STAR GREEN as well as Alexa 568. STAR RED was imaged with excitation at a wavelength of 640 nm and time-gated fluorescence detection between 650 and 760 nm. STAR ORANGE and Alexa 568 were excited at 561 nm with time-gated detection between 571 and 630 nm for STAR ORANGE and 573 and 683 nm for Alexa 568. STAR GREEN and FITC were excited at 488 nm with time-gated detection between 498 and 551 nm. The Abberior MATRIX array detector was used to reduce unspecific background signal. The STED lasers had a wavelength of 775 nm and a pulse width of roughly 500 ps. An oil-immersion objective was used (UPLXAPO 60XO, NA: 1.42, Olympus, Japan).

For assessment of PDFGRβ+ cells to total cells in confocal images, regions of interest were arbitrarily placed over the selected cortical compartments. Labeled cells with a DAPI-positive nucleus in the optical plane were individually marked in the "3D-environment" function of Neurolucida 360 software and calculated per mm^2 and per mm length of blood vessels, respectively. Data management was done in Microsoft Excel 365. All graphs were made with SigmaPlot 12.3 (Systat Software GmbH).

The reconstruction and evaluation of blood vessel data was done with the Imaris 10.1. software (Oxford Instruments). Regions of interest were arbitrarily placed over the selected cortical compartments. *Z*-stacks were mostly in the range of 100–200 µm, limited either by microscopic range, computing power, and, in few cases, depth-depending fading of antibody staining. First, a semi-automatic layout of the 3D vessel pattern was generated with the "filament" algorithm. Next, manual corrections were done such as deleting redundant or adding missing parts and branch points and correcting vessel thickness. The two litters aged E68 and E72 were combined under E70; E100 data were pooled with data from E110 because the two were not different. Statistical measures were taken from Imaris, data management was done as described above. A major technical consideration concerns the automated data acquisition from digital images promised by the software tools. In our case, the tools deliver a coarse layout of the vessel pattern but that requires a serious workover by trained examiners because, for example, thin vessel connections would have been missed. A similar note toward involving the best hightech available, the human retina and brain, has been given for working with automated serial reconstructions of EM images (Shapson-Coe et al. 2024; Wu et al. 2024).

Protein blots were photographed, and relative band intensities were determined with ImageJ. All protein bands were normalized to the 42 kDa β-actin or the 55 kDa β-tubulin band, which served as control for loading equivalency. Values were normalized to the P90, which was considered adult. For every protein, at least three independent lysates from cortex of two animals (mostly from the same litter) were tested for every age.

3 | Results

3.1 | The Early Phase of Angiogenesis

Stage E45 is shortly after the transition from embryonic to fetal in pig, the hippocampal *anlage* is recognizable, and the stage is comparable to 15th/16th gestational week in human (Meyer 2010). Examination of occipital cortex and midbrain (Figure 1A) revealed a dense and very uniform network of vasculature in the midbrain *anlage* (Figure 1B), whereas only very few vessels can be seen in the cortical *anlage* (Figure 1C,D). Large and small diameter vessels were present in the meninges (Figure 1C, inset C1), and vessels are innervated by Neuropeptide Y-positive fibers (Ernst et al. 2018). At E45, gyrification had not yet begun and the transient cortical layers such as cortical plate (CP) and subplate (SP) were narrow in depth. Intermediate zone (IZ) and ventricular zone (VZ) occupied about two-thirds of the cortical depth (Figure 1C, inset of a thionin-stained panel) and most of the vessel elements were within the proliferative VZ/SVZ presumably to supply the stem cell niche. Vessels within the outer layers were mostly unbranched, while those in VZ/SVZ had already developed some branches and anastomoses (Figure 1D, inset D1). No preferred orientation of the vessels could be recognized. In the IZ, as well as the SP, CP, and marginal zone (MZ), the vessel density was low. This qualitative observation suggests a high angiogenic activity at the begin of fetal development. The substantially advanced microvessel pattern in the midbrain matched well with the finding of numerous microglia cells and oligodendrocyte progenitors reported earlier for the midbrain *anlage* (Sobierajski et al. 2022; Sobierajski et al. 2023).

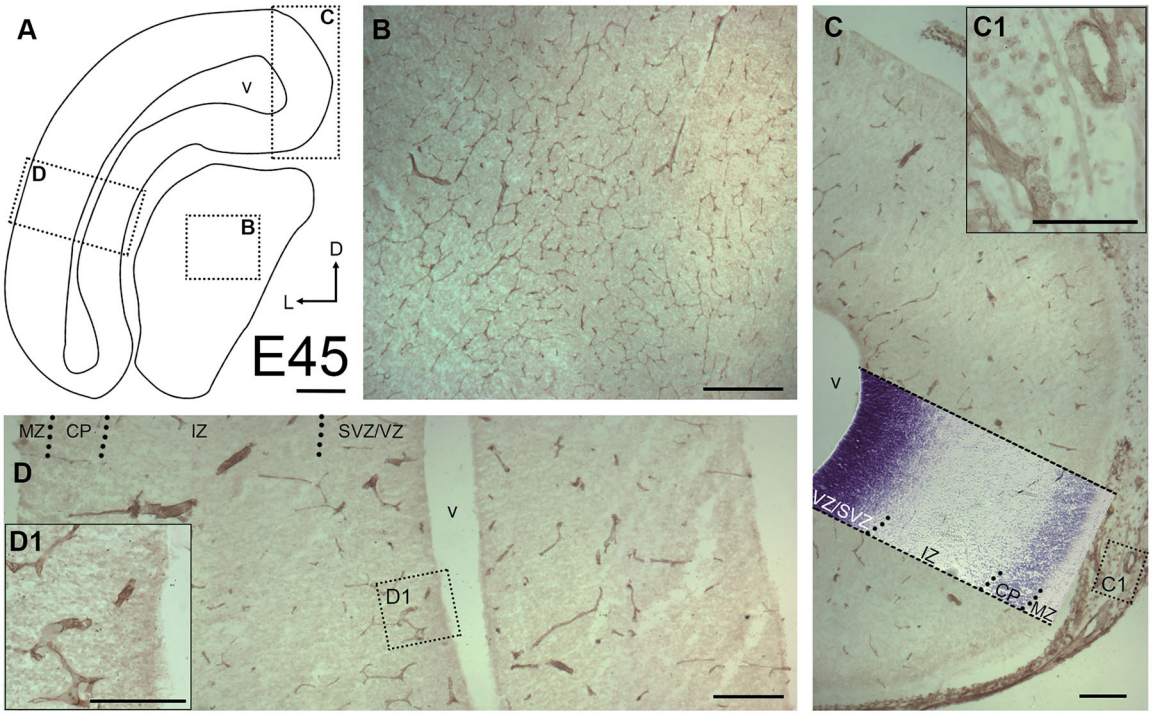

FIGURE 1 | Qualitative assessment of blood vessels at E45. (A) Outline of a section through occipital cortex and midbrain *anlage*. Arrows: D, dorsal; L, lateral. Boxed regions are shown at higher magnification in the insets. (B) The midbrain *anlage* already displayed a dense vascular network, which was stained with tomato lectin. (C) Cortex, medial aspect. A thionin-staining panel has been overlayed to demonstrate the laminar compartments. Meninges have been partially left attached to avoid damaging of the cortex. (C1) The meninges displayed a dense network of thick and thin vessels. (D) Cortex, lateral aspect. The developing upper layers display hardly any vessels while VZ/SVZ display more vessels. *Abbreviations* (apply to all following figures): MZ, marginal zone; CP, cortical plate; IZ, intermediate zone; SVZ, subventricular zone; VZ, ventricular zone; v, ventricle. Scale bars: 200 μm in A–D; 100 μm in D1.

3.2 | Midfetal to Postnatal Stages

Next, individual gyri of the VC at E70 to P90 were imaged (Figure 2). A massive increase in vascular density has occurred compared with E45. Given the enormous expansion of the pig brain and cortex (Ernst et al. 2018), we selected a major gyrus at E70 and successively smaller gyri at E85 and E100 in order to show the patterns roughly at the same magnification. As an example of the laminar expansion, the thickness of MZ/layer 1 (L1) increased dramatically from E70 to E100 (from ~123 to ~385 μm; measured midlevel at gyral flanks; see Figure 2A1,C1). The gray matter (GM) thickness (border of MZ/L1 to border of white matter (WM)) measured at the same position increased from ~540 μm at E70 to ~890 μm at E100. At E70, long, unbranched vessels extended from deeper WM toward the apex of the gyri (Figure 2A). Thinner branches bended off and extended through the GM layers and connected to vessels that penetrate the MZ/L1 from the pial surface. All vessels formed thinner branches on their way through the cortical layers, which are commonly referred to as penetrating arterioles. GM layers, in particular the cell-dense CP, were only sparsely covered by vessels.

At E85, vessel density had increased forming a seemingly homogeneous network in all layers of the GM (Figure 2B) with higher numbers of penetrating arterioles. The pattern at E100 differed in that the density of finer capillaries had increased in GM and L1 accompanied by an increased density of penetrating arterioles (Figure 2C). The vascular density of deeper layers and WM had changed less compared with E85. At P90 (Figure 2D), the vessel density had again increased visibly as compared with E100 suggesting that the angiogenic activity remained high after birth.

3.3 | Development of the Vascular Network in the Cortical Compartments

During embryonic development, the vascularization of the telencephalon is driven by two plexi, the periventricular vascular plexus and the perineural vascular plexus, which is wrapped around the developing CNS (Kaushik et al. 2020; Kurz et al. 1996; Penna et al. 2021). The perineural vascular plexus runs along the pia mater and grows specialized tip cells, which enter the MZ/L1 perpendicularly. This way regularly spaced vertical vessel trunks emerge. Tip cells direct the sprouting vessel very similar to how growth cones steer elongating neurites. Proliferation of endothelial cells delivers the material for the vessels and the penetrating arterioles, and finally capillaries.

For a quantitative assessment, a linear measure of the surface has been taken at arbitrarily selected positions. The number of vertical vessel trunks was determined (Figure 3A–C). Furthermore, number of vessels crossing the border of MZ/L1 to CP/GM was counted as a readout for the branching within the MZ (Figure 3D). On average, at E70, 15 penetrating vessels per 1 mm surface were counted at the pial surface, and 24 vessels/mm were counted at the CP/GM border. At E85, 19 penetrating vessels/mm at the pial surface, and 21 vessels/mm were counted at the CP/GM border. At

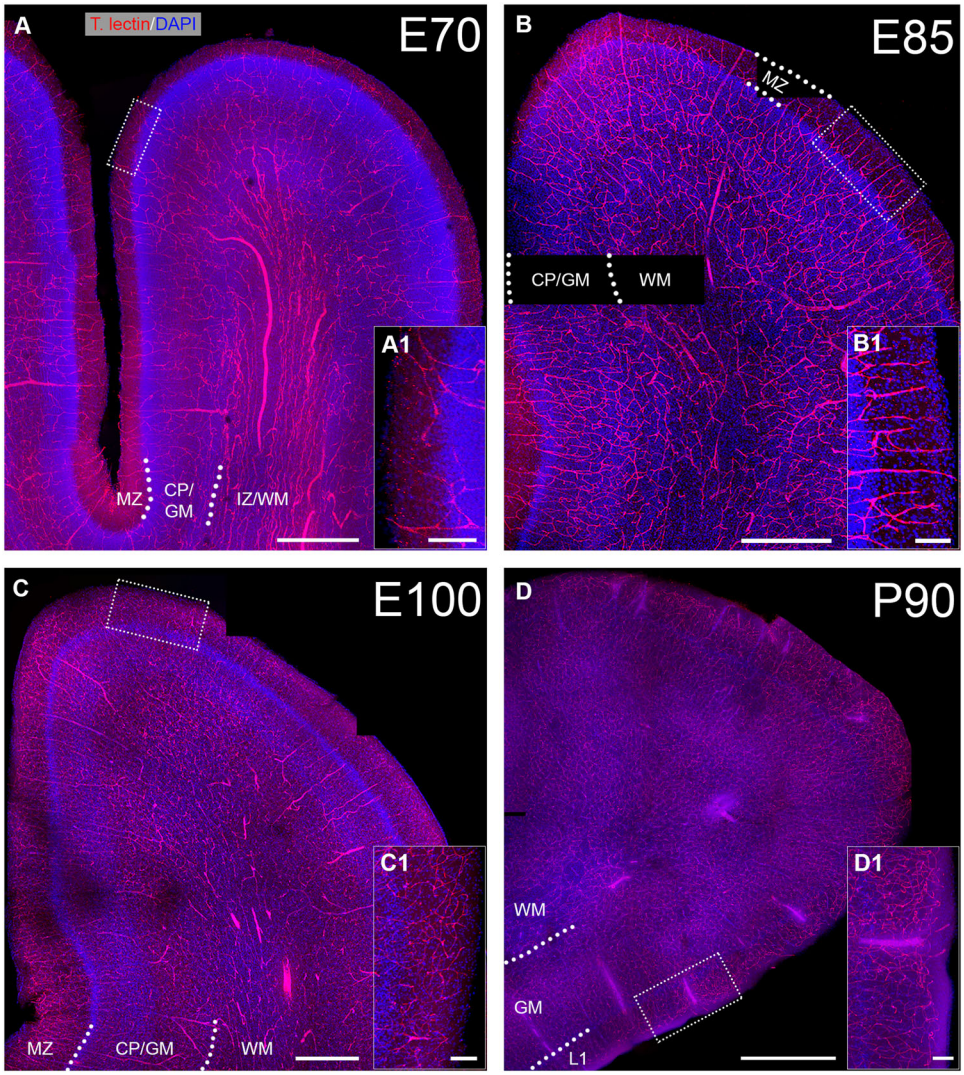

FIGURE 2 | Blood vessel pattern from E70 to P90. Cleared brain sections of ~300 µm thickness were stained with Tomato lectin to visualize blood vessels (red). Nuclei were stained with DAPI (blue). Selected gyri of visual cortex were imaged with tile scans. (A) E70, note the long unbranched vessels with large diameter in the IZ/WM. (B) E85, larger numbers of perpendicular vessels can be seen that branch in the CP/GM. (C) E100. (D) P90. (A1, B1, C1, D1) For every age, a magnification of apical MZ/L1 is shown to compare the thickness of L1 as well as vascular density. Scale bars: 500 µm in A–C, and 1000 µm in D; 100 µm in A1, B1, C1, D1.

E100, 27 penetrating vessels/mm were counted at the pial surface, and 39 vessels/mm were counted at the CP/GM border. Together, within a period of 30 days the number of penetrating vessels doubled and many appear to branch within the MZ/L1 concurrent with the substantial increase in brain volume (Ernst et al. 2018).

Next, a quantitative assessment of vessel densities in cortical layers was done to assess the progression of angiogenesis. For this purpose, cleared slices of approximately 300 µm thickness were stained with immunofluorescence, imaged, and analyzed with the Imaris software (workflow is shown in Figure 4A). The VZ is a transient cell layer. It decreased substantially between E100 and P30 in pig and was therefore excluded at P30. Source data of all assessed parameters shown in Figures 4 and 5 are available upon request.

First, we measured the volume occupied by blood vessels in relation to the total volume of the sample (Figure 4B). Vessels gradually obtained more total space in GM layers while vessel volumes in SVZ/VZ remained comparatively low throughout development. A maximum of ~3.0% vessel volume of total sample volume was reached in the CP/GM around E100 and remained until P30. In the IZ/WM, vessel volume was at a stable level of ~2.35% at E70 and stagnated until P30. Interestingly, at the border between VZ and ventricle, nearly no vessels could be found (Figure 5A). This zone has been described to harbor an avascular niche for the apical neural progenitor cells, which reside in contact with tip cells of vessel sprouts (Komabayashi-Suzuki et al. 2019).

Interestingly, readouts for vessel volume, branching, and vessel length per volume of the domestic P5 were somewhat lower than the E100/110 in the MZ/L1 and mainly in CP/GM (Figure 4B,C,D). This might suggest that vascular development in domestic pig tends to proceed slower or to remain below the measures reached by wild boar individuals.

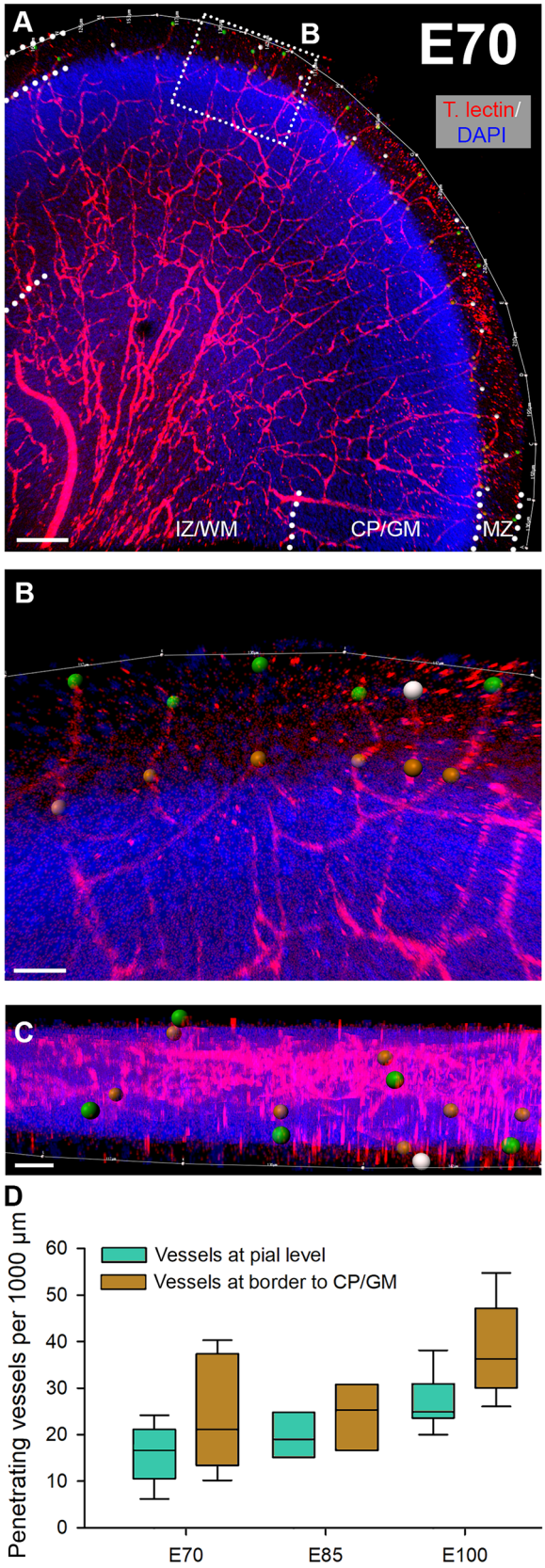

FIGURE 3 | Penetrating blood vessels in visual cortex. From E70 to E100, the number of penetrating vessels that enter from the pial surface were plotted. (A) Tomato lectin-stained gyrus at E70. The dotted rectangle is magnified in B. (B) The pial surface length was outlined (thin white line) and measured. Green dots represent vessels at their entrance positions into the cortex. Gray dots represent vessels for which the entrance point could not exactly be determined due to leaving the *z*-axis of the confocal stack (at least 200 µm depth were imaged). Yet, it was reasonable to assume they might have also entered from the pial surface. Brown dots mark vessels that cross the MZ/L1 to CP/GM boundary. (C) *Z*-view of the region of interest shown in B. (D) Quantitative assessment of penetrating vessels at pial level and at level of MZ/L1 to CP/GM border. Nuclei were costained with DAPI. Scale bars: 150 µm in A; 40 µm in B; 80 µm in C.

In addition, the average diameter of vessel segment was determined (Figure 5B). The largest vessel diameters were measured in the IZ/WM (4.88–6.71 µm) and SVZ/VZ (4.89–5.92 µm), followed by the CP/GM (3.58–5.11 µm) and MZ/L1 (3.03–4.87 µm) with smaller vessels on average. Vessel diameter did not change much in MZ and CP/GM from E70 to E100, and only subtly increased at postnatal age.

Second, the number of branching points per 100 µm vessel length was determined (Figure 4C). A maximum vessel branching seems to be reached in the GM shortly before birth with 1.18 branching points/100 µm at E100, then declining slightly and stabilizing postnatally. Overall lower branching was seen in IZ/WM and SVZ/VZ.

Third, the total length of the reconstructed vessels per volume was measured in mm per mm^3 (Figure 4D). The vessel length matches the results of the relative volume occupied by blood vessels and follows a similar development, as expected. Again, the CP/GM displayed the highest density with 733 mm per mm^3 at E100. Likewise, the average vessel length in the SVZ/VZ was the lowest of all cortical layers.

Fourth, the average blood vessel segment area was determined (Figure 4E). A segment was defined as the part between two branching points. Both, in MZ/L1 and CP/GM, the segment area displayed only minor fluctuations. The largest change occurred in IZ/WM. Here, the average vessel area was initially 3–4-fold higher than in GM, only to decline substantially at E100 to a plateau persisting until P30. A similar picture can be observed in the data of the average segment volumes and segment lengths (Figure 5C,D). Compared with MZ/L1 and CP/GM, there were fewer vessels in the deeper cortical compartments WM and SVZ/VZ. This finding increased the relative influence of individual large vessels occasionally encountered in the arbitrarily selected ROI. It explains the overall higher *SEM* of the statistical analysis. Also in human and rhesus monkey, the vessel density declines toward the WM (Lauwers et al. 2008; Weber et al. 2008).

3.4 | Establishment of BBB Cellular Components

The BBB becomes gradually assembled (Daneman et al. 2010). Here, we analyzed time of appearance of major structural and molecular components of the BBB (Figure 5). Essential for barrier function are astrocytes whose end feet are ensheathing capillary vessels contributing to the membrana limitans gliae perivascularis this way (Haug 1971). At E45, the considerable differences described above (Figure 1) between the midbrain *anlage* and the cortex can again be observed (Figure 6A–D). Astrocytic end feet immunopositive for the water transporter

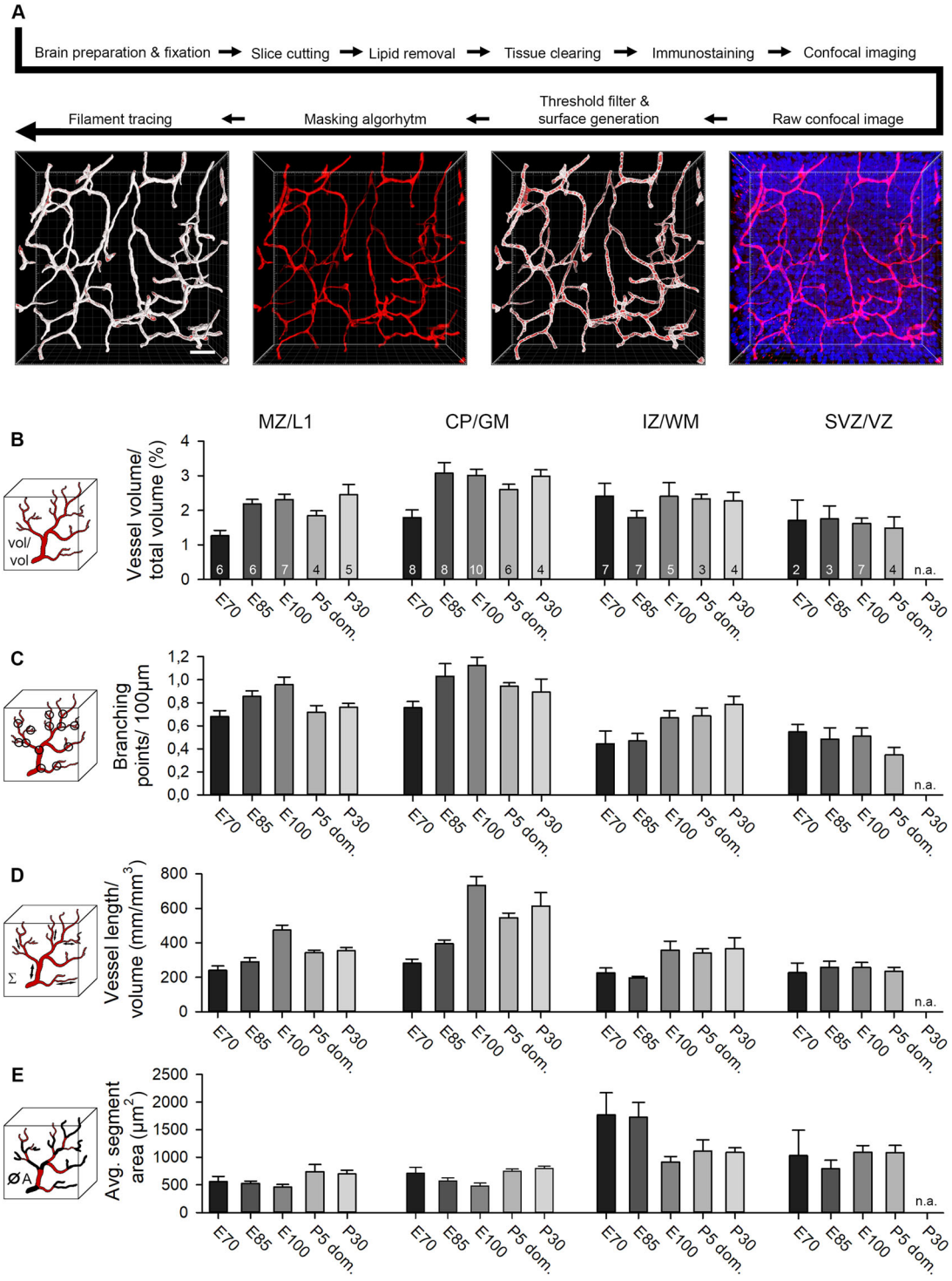

FIGURE 4 | Quantitative assessment of vasculature. (A) Experimental workflow from dissection to filament tracing (Imaris). The raw confocal image was processed with a threshold filter and a masking algorithm. Next, the "surface" tool was used to create a surface for volume measurement and masking algorithm. The "filament" tool yielded a semiautomatic layout of the vessel pattern, which has in all cases been manually refined. Vascular parameters were addressed in four laminar compartments. If present, the SP was included in the IZ/WM compartment. (B) Volume of all vessels compared with the total sample volume. (C) Vessel branching points were calculated per 100 µm. (D) The length of vessels was set in relation to the total sample volume. (E) The average vessel segment area. Vessel sections between two branching points were defined as segments. The numbers in the bars represent the number of nonadjacent regions of interest that were assessed for this compartment. At P30, no sufficient SVZ/VZ area could be found suitable for reliable reconstruction of that compartment. n. a., not applicable. Error bars represent the mean ± *SEM*. Scale bars: 40 µm in A.

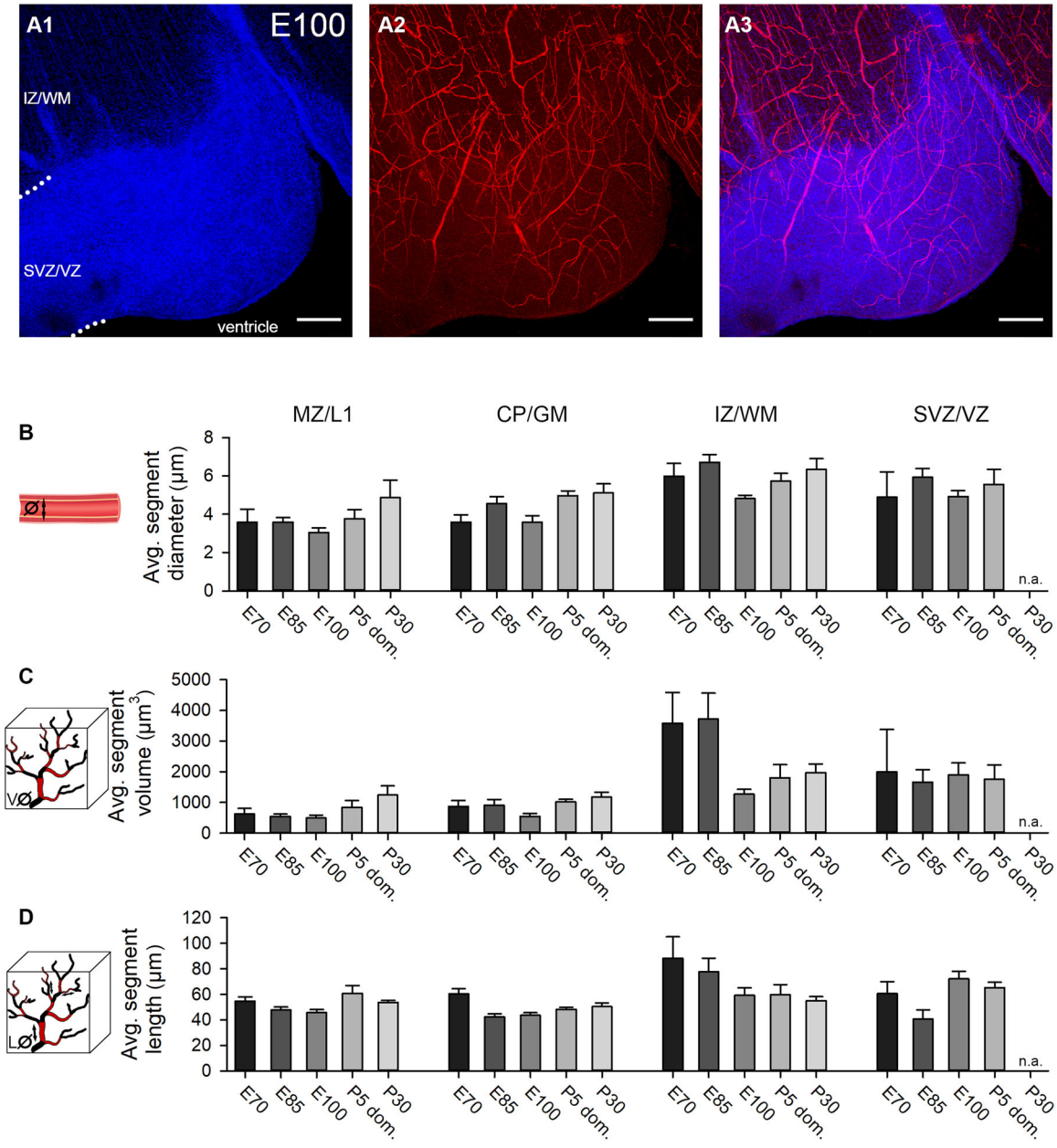

FIGURE 5 | Microvasculature assessment. Tissue processing and data acquisition as described in Figure 4. (A1–A3) Cortex at E100; IZ/WM, SVZ/VZ. In fetal pig cortex older than E60, the VZ is folded into lobes such as the one shown here. Shown are maximal projections of single channels (A1 and A2) and merged channels (A3). At the ventricular border, a narrow zone is sparsely supplied by blood vessels. (B) Average segment diameter of blood vessels. (C) Average segment volume. (D) Average segment length. Error bars represent the mean ± *SEM*. Scale bars: 25 µm in A1–A3.

aquaporin 4 (AQP4) establishing contact with capillaries were present in the midbrain *anlage* (Figure 6A). This contrasted with the situation in the cortical VZ, where astrocytes cannot be found at E45 (Figure 6C), except for first signs of AQP4+ end feet detected close to the lateral ventricle (Figure 6D, small inset). Western blots confirmed the expression AQP4 protein at E65 (Figure 8B). As reported (Sobierajski et al. 2023), lysates have been made from the apex of gyri and thus are enriched for GM. Together, this suggested that vessel-contacting end feet develop first in deep laminar compartments and later in GM. An intact BBB depends on functional tight junctions, which act as physical seal between endothelial cells. Indeed, the tight-junction protein claudin-5 was detectable in capillaries at E45 in deeper cortical compartments suggestive of being the earliest evidence for BBB development.

Structurally, tight junctions of choroidal epithelia cells are present around E60 (~0.41 gestational age) in sheep and at comparable stages in early human fetal brain of 60 mm crown-rump-length (Mollgøard and Saunders 1975). At E60, claudin-5 immunoreactivity was present in all layers suggestive of an existence of stable tight junctions (Figure 6G1–G3,H1–H3). High-resolution STED images of vessels were taken at E68 (Figure 6I1). Here, we show an arteriole with a branching capillary in the cortical GM (Figure 6I2–I6). We defined every blood vessel as a capillary that had a diameter below 8 µm, based on reports that first,

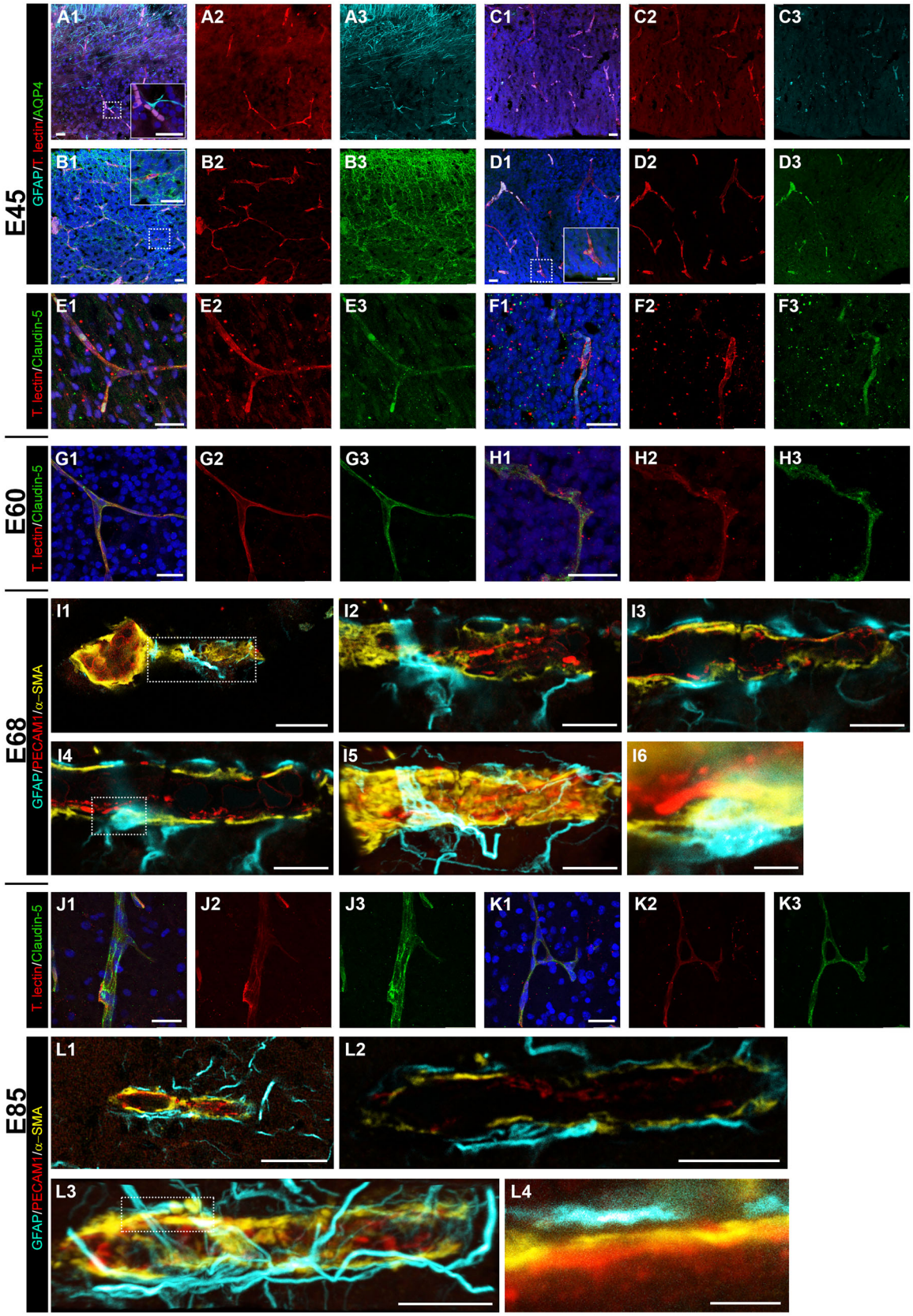

FIGURE 6 | Establishment of the neurovascular unit. (A and B) Midbrain *anlage* at E45. (C–F) Cortex at E45. Shown are maximal projections, merged to the left, next to the single channels. (A and C) GFAP staining (cyan). Note the presence of GFAP+ cell processes contacting blood vessels in midbrain (magnified in the inset). Cortical VZ is still void of GFAP+ cells or processes. (B and D) AQP4+ staining (green). Note glial end feet building a barrier around capillaries in midbrain (magnified in the inset). The cortical VZ is nearly void of AQP4+ end feet. First indications are weakly stained

puncta near capillaries close to the ventricle (magnified in the inset). (E and F) Claudin-5 staining in cortex (green). (E1–E3) Immunoreactive vessels in IZ/WM. (F1–F3) Immunoreactive vessels in VZ. (G and H) Cortex at E60; claudin-5 staining. (G1–G3) Immunoreactive vessels in upper GM. (H1–H3) Immunoreactive vessels in VZ. (I) Cortex at E68; STED images. (I1) An arteriole immunoreactive for PECAM1 (red) with branching capillary in the CP/GM. (I2–I4) Single *z*-stack images at different levels of the vessel shown in boxed region of I1. (I5) Maximum projection, note the layer of α-SMA (yellow) and GFAP+ (cyan) elements partially ensheathing the blood vessel. (I6) Astrocytic cell body closely attached to the blood vessel; magnified from boxed region of I4. (J and K) Cortex at E85. (J1–J3) Claudin-5+ penetrating arteriole in CP/GM. (K1–K3) Claudin-5+ vessel anastomosis in IZ/WM. (L) Cortex at E85; STED images. (L1) Thin capillary in the CP/GM. (L2) Single *z*-stack image of vessel shown in L1. (L3) Maximum projection. (L4) Close-up of boxed area of L3. Note the gap between the astrocytic process and the surface of the blood vessel. Nuclei were stained with DAPI (blue). Scale bars: 25 µm in A–H; 20 µm in I1 and L1; 10 µm in I2–I5 and L2–L3; 2 µm in I6 and L4.

the human capillary diameter underlies a Gaussian distribution with a mean of 6.23 ± 1.3 µm (Cassot et al. 2006) and second, around 80% of all vessels are capillaries (Bryant et al. 2023). Images of the individual *z*-layers show the assembly in detail. PECAM1 was mainly expressed on endothelial cells and particularly intensive at the contact points between neighboring cells. The actin isoform α-smooth muscle actin (α-SMA), is known to be expressed in arterioles and capillaries, but also in a significant number of mid-capillary pericytes mediating their contractility (Bandopadhyay et al. 2001). α-SMA forms a layer on top of the PECAM1+ endothelial extensions. The cell body of a GFAP+ astrocyte resided directly on the vessel (Figure 6I4 and I6), and its extensions were wrapped around the vessel (Figure 6G5), albeit not completely ensheathing it (Figure 6I2–I4).

At E85, claudin-5 increased in intensity and more immunoreactive punctae were present along the vessels, suggesting further strengthening of tight junctions (Figure 6J1–J3,K1–K3). The interactions between astrocytes and the vessel wall were even more prominent at E85 (Figure 6L1). The astrocyte network around the vessels was denser with only minor gaps (Figure 6L2,L3). In detail, astrocytic processes established close contact to the surrounded vessel (Figure 6L4).

3.5 | Development of Pericyte Population

Another essential component of the neurovascular unit are the pericytes marked by the expression of the cell surface tyrosine kinase receptor platelet-derived growth factor receptor β (PDGFRβ) (Smyth et al. 2018). Pericytes are crucial for BBB integrity during embryogenesis, and associate with blood vessels before astrocytes appear. *Pdgfrb*$^{-/-}$ knockout mice die at birth (Daneman et al. 2010). In adulthood, they cover about one third of the vascular surface (Mathiisen et al. 2010), and the coverage is important for reducing vascular permeability and immune cell entry (Daneman et al. 2010). Being localized within the perivascular space they regulate blood flow velocity and permeability of the capillaries. Recent studies have revealed a surprising link toward enhancing long-term potentiation via activity-evoked pericytic secretion of insulin-like growth factor signaling (Pandey et al. 2023), which is also an important neurotrophin for neural maturation and survival (Benarroch 2012).

Here, we quantitatively determined the number of PDGFRβ+ cells to gain insight into the distribution and appearance of this cell class (Figure 7). Cells were scored as positive when they had a clear PDGFRβ+ outline and were closely apposed to a blood vessel (Figure 7A,B,C), as done earlier (Whiteus, Freitas, and Grutzendler 2014). Pericytes frequently resided at the branching point of the vessels suggesting a more efficient sphincter effect at such crossings (Figure 7A4,C4). Already at E60, pericytes were found in all cortical compartments, with a maximum density of 10 cells/mm^2 in CP/GM and IZ/WM (Figure 7D1). At E70, the cell density had increased in all layers, mostly in the CP/GM with 22 cells/mm^2 (Figure 7D2). At E85, an average value of 30 cells/mm^2 was determined in the CP/GM, while all other layers were still below 25 cells/mm^2 (Figure 7D3). At E100, the cell count continued to increase in all compartments reaching a maximum density of 52 cells/mm^2 in the CP/GM, with lower densities in the WM and SVZ/VZ (Figure 7D4).

3.6 | Development of Vessel-Related Protein Expression in SC and VC

We previously reported that the SC develops more rapidly than the VC because the expression of myelin-related proteins occurs earlier (Sobierajski et al. 2023). The finding has been interpreted as being due to the advanced development of the specific somatosensory-evoked activity compared with presumably only spontaneous activity from the retina. This led to the question if the expression of proteins related to angiogenesis also differs between the two sensory areas. Protein expression has been quantified in cortex samples from VC and SC, both containing GM and WM of the apex of gyri with material of E65 being the youngest available in our raw material collection (Figure 8). Claudin-5 expression was detectable from E65 onward with increasing intensity (Figure 8A), confirming the immunofluorescence stainings (Figure 6). In sheep brain, expression of claudin isoforms and zonula occludens proteins is detectable from 0.60 gestational age onward (Sadowska et al. 2015), which translates to ~E85 in sheep and equals ~E70 in pig. Moreover, the cerebral vasculature responds with dilation to NMDA receptor-mediated release of nitric oxide as early as 0.65 gestational age in sheep (Harris, Ohata, and Koehler 2008). Expression of AQP4 increased steadily until P90, and the two areas displayed the same expression levels (Figure 8B). α-SMA protein was at the adult level in both areas from E65 onward (Figure 8C). The tight junction protein occludin was weakly detectable in 3 out of 5 independent lysates of E65 of the two areas (Figure 8D). The major band of predicted 63 kDa was present from E85 onward, and expression in SC lysates appeared to be subtly accelerated compared with VC. With increasing age, weak side bands of larger molecular weight appeared, possibly representing posttranscriptionally and/or posttranslationally modified forms of occludin (Cummins 2012). These isoforms were not included in our quantification. The PECAM1/CD31 antibody delivered a single band at 130 kDa (Figure 8E). In the younger stages from E60 to E85, the average band intensity was low, it started to increase at

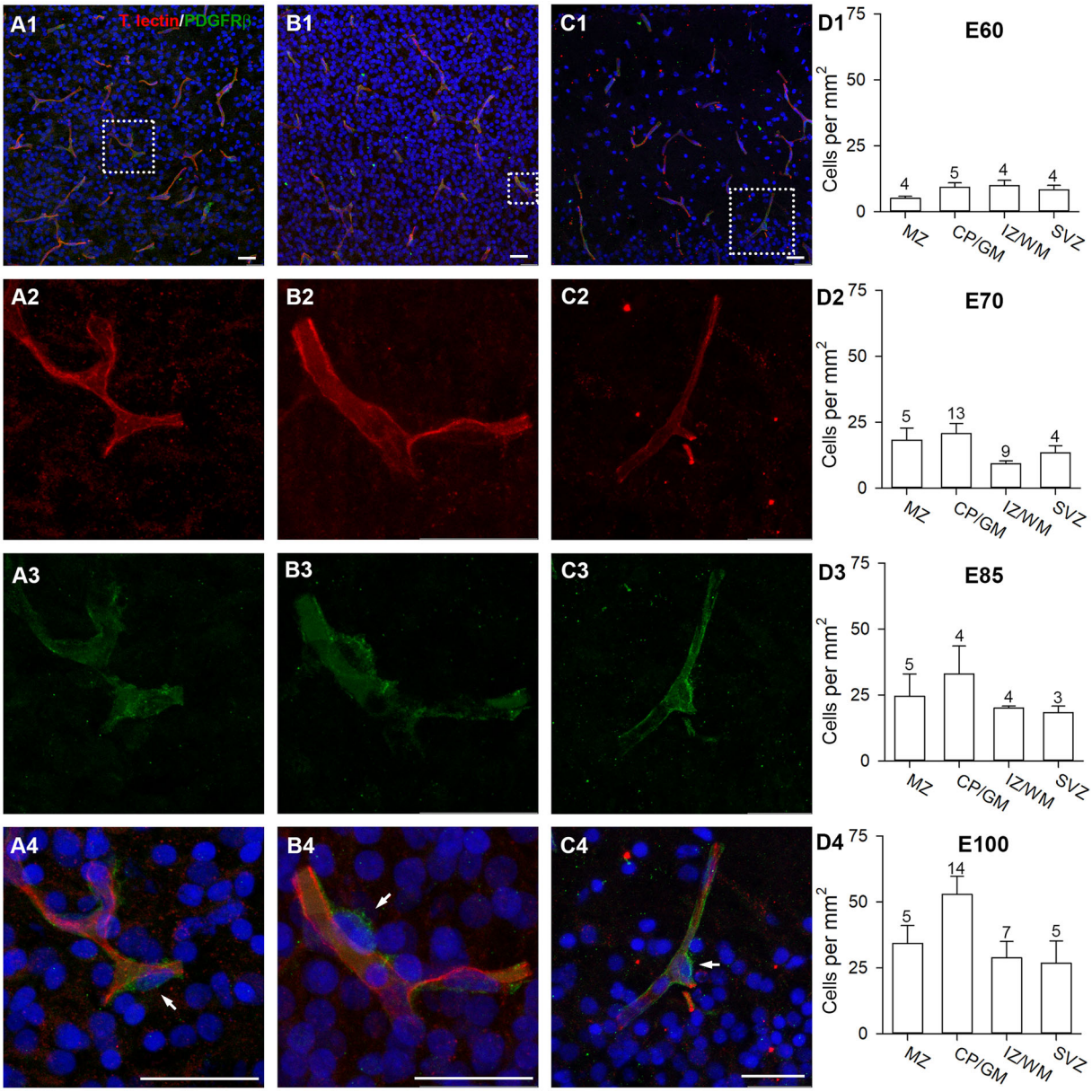

FIGURE 7 | Development of pericytes. Cortex sections were stained with tomato lectin (red) and PDGFRβ (green). PDGFRβ+ pericytes were plotted in ROI selected by the criterion that every ROI contained at least one pericyte. (A1) E60; vessels in L5/6. (A2–A4) Magnification of dotted rectangle in A1 showing the single channels and merged. Pericytes (white arrows) were identified as PDGFRβ+ cells forming "bulges" along the vessels. (B1) E70; vessels in CP. (B2–B4) Magnification of dotted rectangle in B1 showing the single channels and merged. Pericytes have small roundish somata, which differ from elongated somata of endothelial cells. (C1) E100; vessels in the MZ/L1. (C2–C4) Magnification of dotted rectangle in C1 showing the single channels and merged. Pericyte cells often occupy the branching points of blood vessels. (D1–D4) Quantification of pericytes from E60 to E100, mean ± *SEM*. Numbers above the bars report the *n* of ROIs assessed per laminar compartment. Nuclei were stained with DAPI (blue). Scale bars: 25 μm.

E100, and increased further until P90. The cell adhesion molecule vascular endothelial cadherin (VE-cadherin) was well present at E60 followed by a subtle increase until P90 (Figure 8F). Finally, comparing only the P90 values obtained for the proteins in VC and SC (corrected for β-actin) did not reveal differences between the two areas. Taken together, the expression of angiogenesis-supporting proteins proceeded almost concurrently in two cortex areas.

3.7 | Microglia Migrate Through Capillaries and Interact With Vasculature

As a final component of the neurovascular unit we looked at microglia, the development of which has been quantified previously (Sobierajski et al. 2022). Cells of mesodermal origin colonize the embryonic neuroepithelium as early macrophages, and later differentiate into microglia (Hoeffel and Ginhoux 2018). This

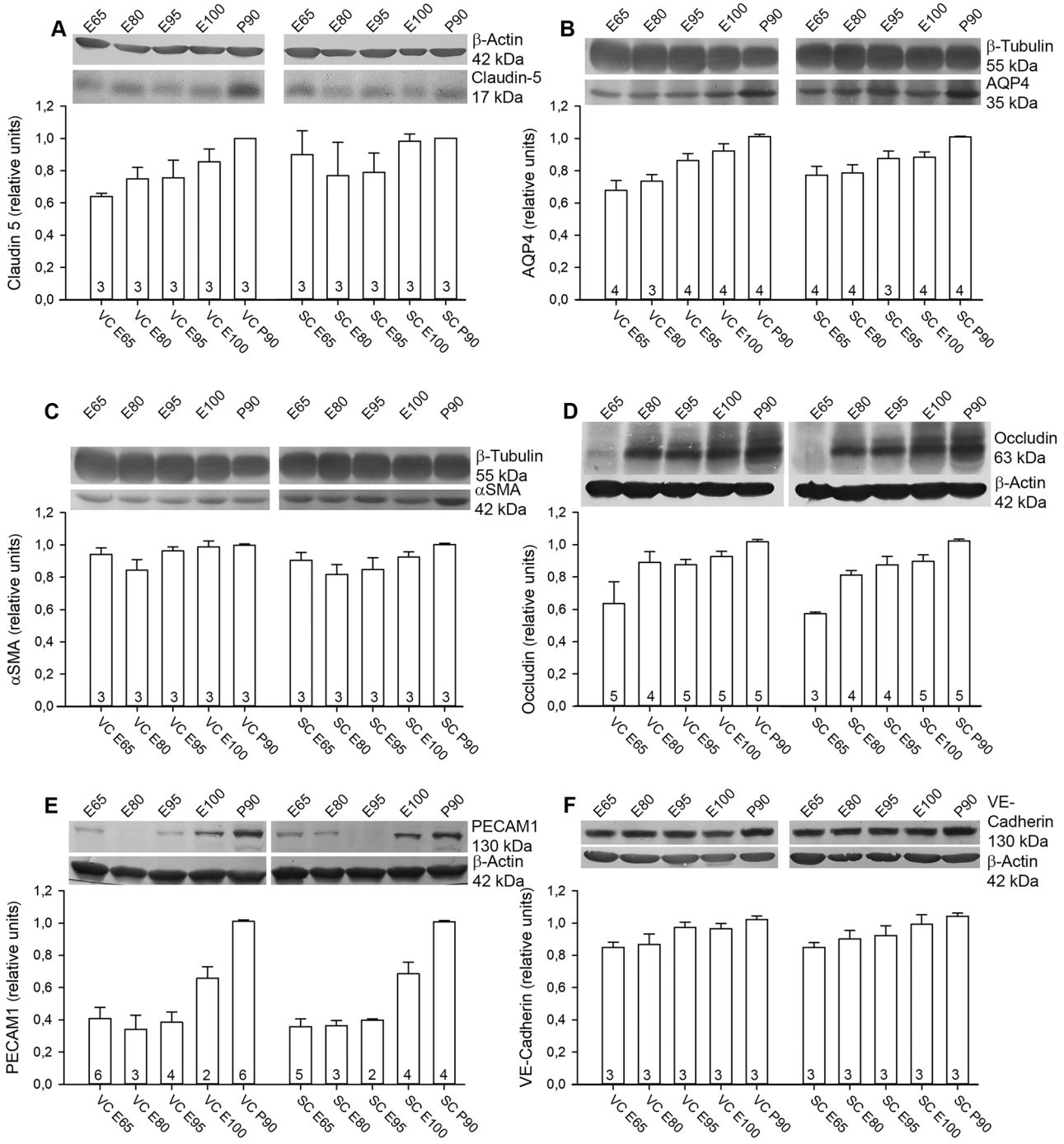

FIGURE 8 | Development of angiogenesis-related proteins. Quantification at E65, E80, E95, E100, and P90 is shown together with representative blots. Visual (VC) and somatosensory (SC) cortex lysates were always run on the same gel to document the area-specific expression profiles. Proteins were normalized to the housekeeping protein *β*-actin or *β*-tubulin as indicated. Normalized protein levels were expressed relative to the amount at P90, which was considered adult, and has been set to 1. (A) Expression of claudin-5. The 17 kDa band was detected from E65 onward. (B) Expression of AQP4. A 35 kDa band was present at E65 and amounts continuously increased during development. (C) Expression of *α*-SMA at 42 kDa was at near adult levels from E65 onward. Note that blots shown in B and C are derived from the same gel and therefore display the same *β*-tubulin band as control. (D) Expression of occludin; only the 63 kDa isoform was quantified. Several other bands with larger size appeared with ongoing development. (E) Expression of PECAM1 was very low at early ages, gaining intensity at E100. (F) Expression of VE-cadherin. A band at the predicted size of 130 kDa was detectable from E65 onward in lysates of both cortices. The numbers in the bars report the number of independent lysates. Error bars represent mean ± *SEM*.

happens before the formation of the BBB is complete. Microglia play important roles, for example, for phagocytosis, synaptic pruning, myelination, and immune surveillance. Recently, it has been shown that microglia cooperate with astrocytes toward phagocytosis of apoptotic cell bodies and neurites (Damisah et al. 2020).

Using ionized calcium-binding adapter molecule 1 (Iba1) as a marker we found round to elongated Iba1+ cell bodies without protrusions within cortical capillaries at E45 in VZ (Figure 9A1–A4) suggestive of monocyte immigration. Such presumably immigrating cells were observed up to E85 and throughout all laminar compartments (Figure 9C1–C4). Microglial cells were already in close contact with blood vessels at E68 and extended their processes closely along the capillaries (Figure 9B1,B2). During development, the more immature microglial cells are partially IB4+. With maturation toward a fully ramified morphology the IB4 reactivity decreases (Wu et al. 1994). This decline can be recognized in pig between E68 and the E85 stage, the latter containing much more ramified microglia (Sobierajski et al. 2022). However, the punctate IB4+ material associated with Iba1+ microglial cells could also be caused by phagocytosis, since microglia cells contribute to vascular remodeling (Alvarez-Vergara et al. 2021), which is expected to happen more frequently at younger stages. At E85, these close interactions were observed more frequently (Figure 9D), and individual processes were wrapped precisely around the vessels (Figure 9D1–D3) and rarely contained IB4+ puncta (Figure 9D2). This suggested that microglia cells monitor the functionality of the BBB. At P90, the number of microglia observed on and around blood vessels had increased substantially and the cells formed patchy networks around the vessels (Figure 9E1–E4).

4 | Discussion

The present study delivers a qualitative and quantitative assessment of the fetal and postnatal development of cerebral cortical vasculature using image analysis of cleared cortex sections and protein blots of two primary sensory areas. At E45 (39% of gestation) a dense network of capillaries could be identified in the midbrain *anlage*, whereas in the cortex primarily layers with high proliferative activity such as the VZ and SVZ already displayed branched capillaries. Penetrating vessels were observed rarely at E45 but more frequently from E70 on. A rapid remodeling then lifted the complexity of the blood vessels network to a near-adult level at E100/110. Additionally, angiogenesis and tight-junction related proteins were expressed at E65 (youngest available) and likely earlier.

4.1 | Species Comparison of Vascular Anatomy in Cortex

Several previous publications have already delivered quantitative data pools, mostly focusing on rodent models of brain insults or young-to-adult transgenic mice harboring disease-mediating gene mutations. The pig is of interest as translational model for neurological disorders, most of which are hitherto considered to have neurodevelopmental origins, and many of which manifest early with vascular problems (Ishihara, Takata, and Mizutani 2023; Ouellette and Lacoste 2021). As an example, amyloid deposits in microvessels emerge before large plaques appear (Take et al. 2022). Extensive data on fetal and early postnatal development are sparse. Comparisons between studies remained difficult because standard protocols for quantitatively assessing angiogenesis are lacking, and therefore, research teams developed their own procedures up to algorithms and modeling. Further, age, breeding lines, sex, and the cortex area or cortical layer examined varied between studies.

To compare the measures obtained in pig to those published for wildtype healthy rodent, monkey, and human (Tables 2 and 3), it is also necessary to judge on the variance of data from various sources. Should the variability be enormous and cover the range of the measures obtained in pig, a comparison would not be very meaningful. However, the species comparison revealed rather minor variations (Figure 10) presumably attributable to natural biological variability, as well as differences in methodologies and analysis strategies. Overall, the blood vessel system occupies approximately the same volume in the species analyzed (Figure 10A). Here, the data for mice exhibit the greatest variation, ranging from 0.6 to 3.6% of the volume. The fractional vascular volume ranges between 2 and 3% in monkey, human, and pig. In neonatal monkey at P2–3 this value is not yet reached, as it is approximately 1%. Moreover, the blood vessel density in relation to the cortical layers is comparable in all species described. There is an overall greater vascular density in GM than in the WM, with highest density in GM layers 5 and 6 (Lauwers et al. 2008; Wu et al. 2014). However, anatomical differences exist (summarized in Figure 11). The density of vessels in rodents is 1.5–2 times higher compared with density in monkey and human (Figure 10B), and pig has a density similar to human. Vessel segment length in rodent is much smaller on average than segment length in pig or human (Table 2). In contrast, the average vessel diameter ranges between 4–5 μm in postnatal rodent and 4–6 μm in E85/P30 pig (Figure 10C), whereas vessels of postnatal monkey and human cortex have larger diameters of 7–10 μm.

The greater density and smaller diameter of blood vessels in rodent could be explained by the high relative density of neurons per volume in rodent cortex compared with human cortex. The neuronal density in mice is 0.6×10^5 to 1.6×10^5 neurons/mm^3, accounting for approximately 40–75% of all cortical cells (Bass et al. 1971; Herculano-Houzel, Mota, and Lent 2006; Irintchev et al. 2005). The neuronal density in human is approximately 0.1×10^5 to 0.5×10^5 neurons/mm^3, which is substantially lower than in rodent (Gittins and Harrison 2004; Gredal et al. 2000). A recent EM study reports that the percentage of neurons in human cortex is 40–65% in L2–L4 and 20–30% in L5–L6 (Shapson-Coe et al. 2024). A neuronal density of 0.2×10^5 neurons/mm^3 is reported for pig VC, which is comparable to that of human (Cragg 1967). Our data confirm that in P90 pig VC NeuN immunoreactive neurons of all cells are approximately 38% in L2–L4 and 22% in L6 (Sobierajski et al. 2022).

4.2 | Assembly of the BBB in Cortex

An important question is when the BBB becomes established. A frequently used method has been the injection or perfusion of tracer molecules such as horseradish peroxidase or serum albu-

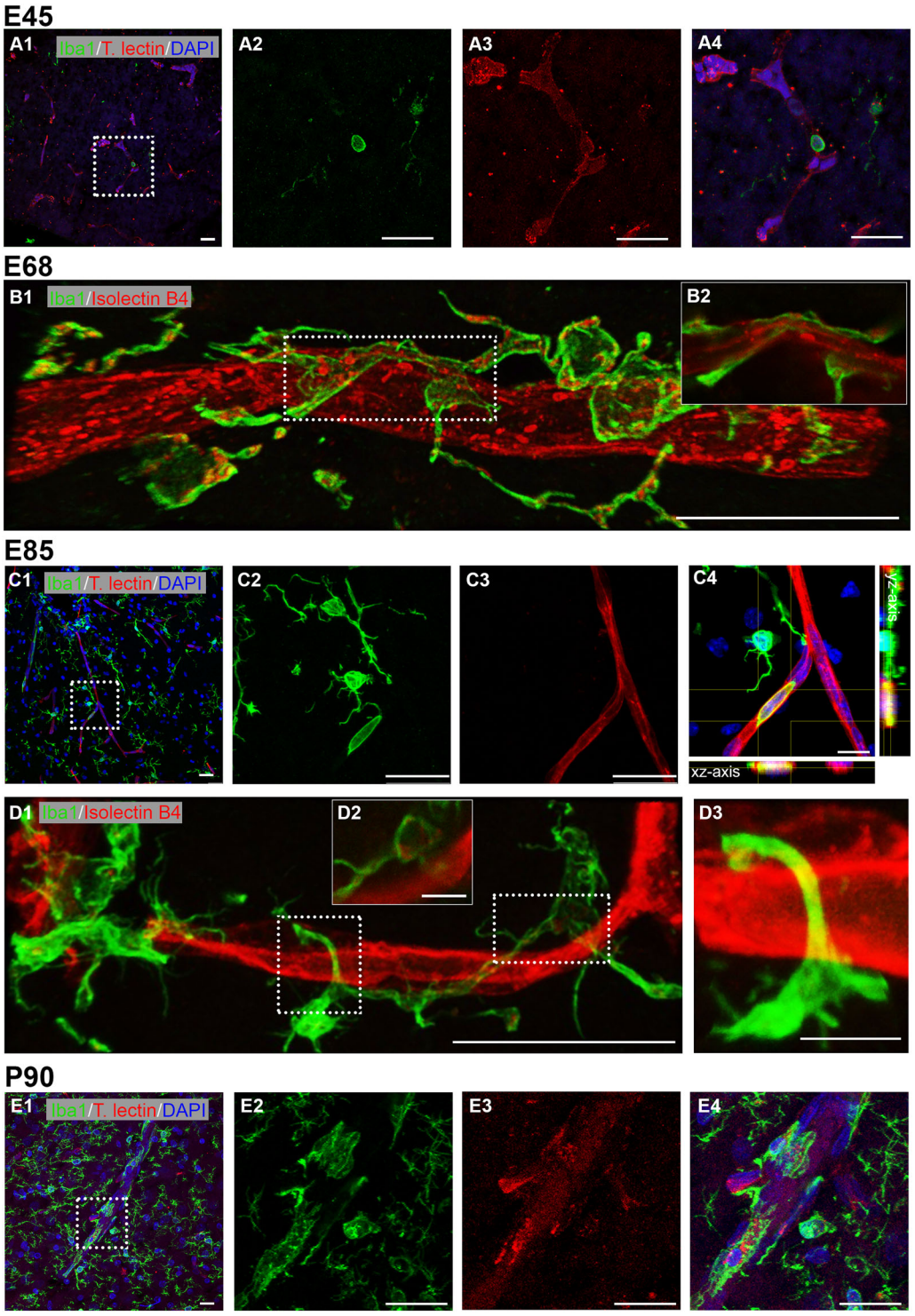

FIGURE 9 | Interaction of microglia and blood vessels. Microglia has been detected with Iba1 (green). Vessels are either stained with tomato lectin or IB4 (red). Microglial cells are also partially IB4+ in particular in more immature stages. (A1) Cortex at E45; labeling in VZ. First Iba1+ cells were visible, showing no to few protrusions. (A2–A4) Single channels and merged of boxed region in A1 shown at higher magnification. A single microglial cell seemed to emerge from a capillary. (B1) Cortex at E68; labeling in GM. Microglial cell wrapping around a vessel. (B2) Single *z*-plane of the boxed region demonstrating that the microglial cell contacts the vessel membrane. Note the frequent association of IB4+ puncta within the Iba1+ microglia, which had not yet acquired a fully mature ramified morphology. (C1) Cortex at E85; labeling in MZ/L1. (C2–C4) Iba1+ monocyte residing inside a blood vessel, as confirmed by *xz* and *yz* axis views. (D1) Cortex at E85; labeling in L5/6. (D2) Single *z*-plane of the right boxed region in D1, indicating weakly labeled IB4+ puncta associated with the microglial cell. (D3) The left boxed region at higher magnification shows a microglial extension wrapping around a vessel. (E1) Cortex at P90; microglia–vessel association in the GM. (E2–E4) Single channels and merged of boxed region in E1 shown at higher magnification. Nuclei were stained with DAPI (blue). Scale bars: 25 μm except 10 μm in C4 and 5 μm in D2–D3.

TABLE 2 | Species comparison of quantitative vessel data. For rodent and primates, we aimed at extracting the same parameters analyzed for the pig, and therefore also included developmental data. The focus has been on neocortex. Published data have been obtained from different cortex areas. Either the average is given or, alternatively, the minimum and maximum. If exact values have not been mentioned in the publications, numbers were extracted from the figures. Only data from wildtype/control animals have been considered. Units have been adjusted for comparison. Note that with regard to the term "volume," it has been difficult to extract from the publications what exactly has been analyzed (total brain volume, total cortex volume, total volume of the sample). Empty fields: The parameter has not been addressed or the specific value could not be extracted. For additional information see Table 3.

Species/age		Vessel volume/total/fractional volume (%)	Fractional vessel volume (relative units)	Vessel length/brain volume (mm/mm^3) Vascular length density (mm/mm^3)	Vascular surface (mm^2/mm^3)	Branching points (1/100 µm)	Branch density ($1/mm^3 \times 10^4$)	Branchpoint density ($BrPts/mm^3$)	Segment area/vessel lumen area ($µm^2$)	Segment volume ($µm^3$)	Segment/branch length (µm)	Segment/vessel diameter (µm)	Distance to nearest vessel (µm)	References Internal source
Mouse	E13,5		0.195				16.5		480		13			Hahn et al. 2021; Figure 4
	8 weeks	2.6		880.00									14.1–16.8	Wu et al. 2014; Figure 5
	10–12 weeks			779.7–807.5				6470.7–8670.7			60	4.7–5.1		Hagemann et al. 2024; Figures 2, 4
	12 weeks		0.24				4.8		1490		23			Hahn et al. 2021; Figure 2
	Adult	3.64										2.5–41		Heinzer et al. 2006; Table 1, Figure 4
Mouse, rat	Adult	0.6–1.2		690–1180								4.0–5.0	14.6	Tsai et al. 2009; Figure 13, S3
Pig	E85	2.20		285.11		0.71			904.62	1695.51	52.09	5.19		Current study
	P30	2.58		445.08		0.82			861.42	1451.08	53.06	5.44		Current study
Marmoset monkey	P2–3	0.45–1.61		44–157	1.48–4.06						53.1–75.7	9.60–11.40	28–55	Risser et al. 2009; Table 2
	5–6 years	2.02–4.30		177–377	5.32–11.32						86.2–98.0	8.34–9.88	24–33	Risser et al. 2009; Table 2
Rhesus macaque	Adult	2.03–2.22		437.82–512.03	10.25–11.50							7.15–7.45		Weber et al. 2008; Table 1
Human	20–65 years	2.44		465	5.37						59.4	6.91–7.72		Cassot et al. 2006; Tables 2, 3
	20–65 years	2.39–3.02		411.60–613.17	10.19–12.85							6.47–7.82		Lauwers et al. 2008; Table 1, Figure 2
	12–54 years			141–368								4.44–5.38		Bell and Ball 1985; Table 1

TABLE 3 | Species comparison of quantitative vessel data. Compilation of vessel data including some not considered in Table 2, such as the animal strain and sex, brain area/region investigated, and the methodology.

Species (strain, age and sex)	Quantified vessel data		Area of brain, method	References Internal source
Mouse (C57BL6/6N, E13,5, male)	Branch length (μm)	13	Cortex	Hahn et al. 2021
	Branch radius (μm)	5.6	Intravenously labeling with T-lectin, selective plane illumination microscopy ("ultramicroscopy")	Figure 4
	Branch density ($1/mm^3 \times 10^4$)	16.5		
	Fractional vessel volume	0.195		
	Vessel lumen surface area (μm^2)	480		
Mouse (C57BL/6 and Kunming, 8 week, male)	Vascular fractional volume (%)	2.6	Visual cortex V1 (L I–VI)	Wu et al. 2014
	Microvascular fractional volume (%)	1.0	Motor cortex M1 (L I–VI)	Figure 5
	Vascular length density (m/mm^3)	0.88	Modified Nissl staining, micro-optical sectioning tomography	
	Microvascular length density (m/mm^3)	0.70		
	Distance to nearest microvessel (V1) (μm)	14.1 (L IV)–16.8 (L VI)		
Mouse (C57Bl/6j, 10–12 weeks, male)	Vessel length density (mm/mm^3)	779.7–807.5	Striatum	Hagemann et al. 2024
	Branchpoint density ($BrPts/mm^3$)	5564.8–5953.0	Transcardial infusion of FITC-albumin hydrogel, Lightsheet microscopy	Figures 2, 4
	Terminal point density ($TermPts/mm^3$)	6470.7–8670.7		
	Total vessel length (mm/striatum)	5112.6–5266.8		
	Diameter (μm)	4.7–5.1		
	Branch length (μm)	60–65		
	Volume density (mm^3/mm^3)	0.0145–0.0175		
Mouse (NOD Scid Gamma, 12 weeks, male)	Branch length (μm)	23	Cortex	Hahn et al. 2021
	Branch radius (μm)	9.0	Intravenously labeling with T-lectin, selective plane illumination microscopy	Figure 2
	Branch density ($/mm^3 \times 10^4$)	4.8		
	Fractional vessel volume	0.24		
	Vessel lumen surface area (μm^2)	1490		
Mouse (Swiss, C57/BL adult, sex unknown), and Rat (Sprague–Dawley, adult, sex unknown)	Microvascular fractional volume (%)	0.6–0.85	Cortex	Tsai et al. 2009
	Vascular fractional volume (%)	0.7–1.2	Transcardial infusion of FITC-albumin hydrogel, confocal microscopy	Figures 13, S3
	vessel length density (mm/mm^3)	690–1180		
	Vessel diameter (μm)	4.0–5.0		
Mouse (C57Bl6, adult, sex unknown)	Vessel volume/total volume (%)	3.638	Entire brain	Heinzer et al. 2006
	Vessel surface/total volume ($1/mm^3$)	15.6	Vascular corrosion casting, scanning electron microscopy, synchrotron radiation microcomputed tomography	Table 1, Figure 4
	Vessel surface/vessel volume ($1/mm^3$)	428.5		
	Connectivity density (1/mm)	3612		
	Vessel diameter (μm)	2.5–41		

(Continues)

TABLE 3 | (Continued)

Species (strain, age and sex)	Quantified vessel data		Area of brain, method	References Internal source
Marmoset monkey (P2–3, sex unknown)	Vascular volume 10^{-2} (mm^3/mm^3)	0.45–1.61	Motor cortex, visual cortex, somatosensory cortex, infero-temporal cortex, frontal cortex, parietal cortex Intracardial perfusion with barium sulfate, synchrotron X-ray micro-tomography imaging	Risser et al. 2009 Table 2
	Surface (mm^2/mm^3)	1.48–4.06		
	Vascular length (mm/mm^3)	44–157		
	Segment length (mm)	53.1–75.7		
	Mean diameter (mm)	9.60–11.40		
	Mean large vessel diameter (mm)	14.00–16.02		
	Mean distance/any vessel (μm)	28–55		
	Mean ratio large/all vessels	0.36–0.52		
Marmoset monkey (5–6 years, sex unknown)	Vascular volume 10^{-2} (mm^3/mm^3)	2.02–4.30	Motor cortex, visual cortex, somatosensory cortex, infero-temporal cortex, frontal cortex, parietal cortex Intracardial perfusion with barium sulfate, synchrotron X-ray micro-tomography imaging	Risser et al. 2009 Table 2
	Surface (mm^2/mm^3)	5.32–11.32		
	Vascular length (mm/mm^3)	177–377		
	Segment length (mm)	86.2–98.0		
	Mean diameter (mm)	8.34–9.88		
	Mean large vessel diameter (mm)	14.70–15.88		
	Mean distance/any vessel (μm)	24–33		
	Mean ratio large/all vessels	0.23–0.56		
Rhesus macaque (adult, sex unknown)	Vessel volume/total volume (%)	2.03–2.22	Cortex Areas V1-V5 (divided in % cortical thickness) Vascular corrosion casting, fluorescence microscopy	Weber et al. 2008 Table 1
	Vascular length density (mm/mm^3)	437.82–512.03		
	Vascular surface (mm^2/mm^3)	10.25–11.50		
	Vessel diameter (μm)	7.15–7.45		
Human (20–65 years, sex unknown)	Vessel volume/total volume (%)	2.44	Collateral sulcus in the temporal lobe Vascular corrosion casting, confocal laser microscopy	Cassot et al. 2006 Tables 2, 3
	Vascular surface (mm^2/mm^3)	5.37		
	Number of segments ($1/mm^3$)	7826		
	Vessel length (mm/mm^3)	465		
	Segment mean length (μm)	59.4		
	Mean vessel diameter (μm)	6.91–7.72		
Human (20–65 years, sex unknown)	Vessel volume/total volume (%)	2.39–3.02	Collateral sulcus in the temporal lobe (divided in lateral, medial, bottom, top) Vascular corrosion casting, confocal laser microscopy	Lauwers et al. 2008 Table 1, Figure 2
	Vascular length density (mm/mm^3)	411.60–613.17		
	Vascular surface (mm^2/mm^3)	10.19–12.85		
	Distance to nearest vessel (μm)	6.47–7.82		
	Number of segments ($1/mm^3$)	7473.59–14,069.39		
	Volume/surface (μm)	2.1–2.4		

(Continues)

TABLE 3 | (Continued)

Species (strain, age and sex)	Quantified vessel data		Area of brain, method	References Internal source
Human (age range 12–54 years, male and female)	Capillary length density (mm/mm^3)	141–368	Visual Cortex (Area 17, LI–LV/VI) Alkaline phosphatase staining, light microscopy	Bell and Ball 1985 Table 1
	Capillary diameter (μm)	4.44–5.38		
	Arteriole length density (mm/mm^3)	10.8–19.5		
	Arteriole diameter (μm)	13.21–15.64		
Human Postmortem samples, age range 2–42, male and female	Vascular density in cortex (counts/mm^2)	73.7–237.2	Frontal cortex, temporal cortex, occipital cortex CD34 staining, digitizing by scanning	Veersema et al. 2019 Table 2
	Vascular density in white matter (counts/mm^2)	44.6–118.3		

min. By injecting human plasma proteins into the vasculature of a E60 sheep fetus, it has been demonstrated that none of the injected proteins had leaked into the brain, thus, the BBB seemed to be tight and functional at that stage (Dziegielewska et al. 1979). The forebrain of a newborn marsupial, the tammar wallaby (born pea-sized after 27 days), corresponds to the forebrain of a 6-week-old human embryo (Reynolds et al. 1985). Plasma proteins or horseradish peroxidase injected intravenously into newborn tammar wallaby did not penetrate into the brain (Dziegielewska et al. 1988). In the South American opossum, a marsupial born at a very early developmental stage (comparable to an E13 rat) when vessels just begin to form, a <300 kDa tracer does not enter into the brain suggestive of a functional BBB at this very early stage (Ek et al. 2006). In rat, BBB assembly proceeds between E15–17 (Olsson et al. 1968) and in mouse between E13–17 (Risau, Hallmann, and Albrecht 1986; Stewart and Hayakawa 1987). In sheep, tight junctions of choroidal epithelia cells are present around E60 (~0.41 gestational age) and at comparable stages in early human fetal brain of 60 mm crown-rump-length (Mollgøard and Saunders 1975). The time course of human BBB assembly relies on detection of the cellular components of the neurovascular unit. During the second trimester in human all components of the unit are present in the pallium including the cerebral cortex (Crouch et al. 2022). In this ensemble of endothelial and mural cell subtypes including smooth muscle cells, pericytes, and fibroblasts, every cell subtype follows its own developmental trajectory. By the 12th week of gestation in human, occludin and claudin-5 are expressed in the primary vessels (Virgintino et al. 2000). The appearance of tight junction proteins at this time seems to be sufficient to prevent albumin from entering the brain, providing evidence of early functionality of the BBB. By the 18th week of gestation in human, occludin and claudin-5 have staining patterns similar to the pattern seen in the adult.

Astrocytes are essential for BBB maintenance. The differentiation of astrocytes and vascular ensheathing begins during the first postnatal week in rodent, and astrocytes appear later than pericytes (Daneman et al. 2010). In human neocortex, first GFAP+ astrocytes are present at the 18th weeks of gestation (Roessmann and Gambetti 1986). Thus, a certain functionality seems already possible before all components are present, which is probably followed by a "tightening" of the tight junctions and reduction of solute permeability (Hellström et al. 2001). In pig, first evidence of astrocytes ensheathing vessels were seen at E45 in midbrain and at E68 in cortex.

Together, the progression of BBB development in pig can be well compared with that in human. At E45, only the tight junction protein claudin-5 could be detected in midbrain and cortex, suggesting an immature state of the BBB. Around mid-gestation in pig all cellular and molecular components were present in cortex and the expression levels of the tight junction proteins reached near-adult levels shortly before birth.

4.3 | Blood Vessel Development in VC and SC Follows a Common Time Course

Myelin-related proteins show an area-specific time course of expression (Sobierajski et al. 2023) with advanced expression in the SC where the rostrum is represented. We have suggested that

FIGURE 10 | Species comparison between rodent, pig, monkey, and human. Quantitative vascular measurements were collected from the published work cited. Plotted are the mean values. (A) Vascular volume in relation to the total sample volume. (B) Vascular density plotted as vascular length per volume. (C) Diameter of blood vessels. Detailed data can be taken from Tables 2 and 3. Error bars represent the mean ± *SEM*. Adapted from Tsai et al. (2009) and extended.

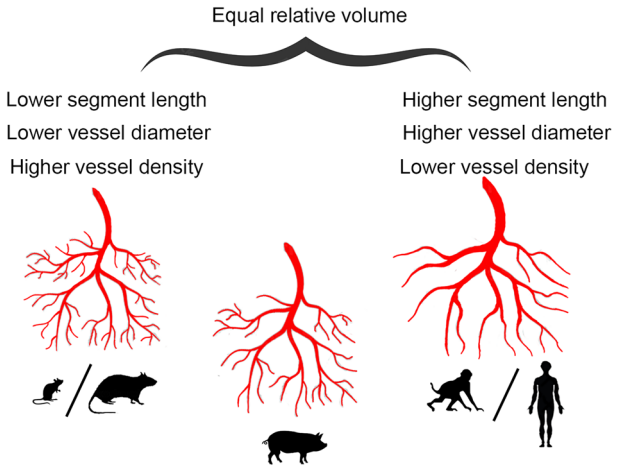

FIGURE 11 | Graphical summary of vessel parameters. Species silhouettes are adapted from Wahle et al., 2022.

this might have been due to somatosensory-evoked activity. This led to the question of whether the vascular development is also advanced in the somatosensory compared with VC. However, we did not observe remarkable differences in expression of angiogenesis-related proteins between fetal VC and SC. This supports the "integrative network" hypothesis, which, based on receptor ligand binding assays in primate brain, claims that cortical fields follow a common developmental trajectory (Lidow et al. 1991). The question is, if such an early onset of angiogenesis might be regulated by neural activity.

In altricial rodent neocortex, a sequence of activity patterns starting with calcium spikes, followed by synchronous plateau potentials, early network oscillations, and giant depolarizing potentials marks the late fetal to early postnatal period (Allène et al. 2008; Luhmann et al. 2016 for review). Around eye opening a P12–14 the early patterns become replaced by sensory-driven activity. A study in P1–P60 rat has revealed areal- and laminar-specific differences in vascular density between visual and auditory cortex and the phylogenetically older entorhinal cortex, but these differences did not emerge before the second postnatal week (Michaloudi et al. 2005). In cat and primate VC, layer 4 in particular develops postnatally an increased vascular density (Fonta and Imbert 2002; Tieman et al. 2004) reflecting the metabolic requirements of the geniculorecipient layer with active vision after eye opening. Whether or not this also occurs in ungulates must be clarified in future work. Currently, we have too few postnatal boar piglets and a causal proof would require an experimental manipulation of postnatal vision.

Spontaneous cortical calcium events have been recorded before eye and ear opening in prematurely born ferret. Moreover, the study has revealed highly similar activity patterns in primary sensory and association cortices with functional networks extending over millimeters suggesting that the initial design of the cortical representations follows the same principle (Powell et al. 2024). Besides spontaneous activity, cortical potentials can be evoked by sensory stimulation at early fetal stages. Visual cortical responses to optic nerve stimulation can be recorded at E55 in sheep (0.37 gestational age, equals ~E45 in pig) as a long-latency surface wave (Persson and Stenberg 1972). The wave pattern is like the wave evoked by somatosensory stimulation at E55, which is discussed to reflect postsynaptic potentials in basal dendrites of cortical pyramidal neurons of infragranular layers and SP (Molliver 1967). Cortical responses to stimulating the snout in fetal sheep can be recorded as early as E97 (gestational age 0.65 in sheep; equals ~E75 in pig) (Cook et al. 1987). Visually evoked potentials can be recorded in sheep from E111 onward (0.75 gestational age in sheep equals ~E85 in pig), and VEP wave forms continue to mature after birth (Woods and Plessinger 1986). Single unit recordings in postcentral cortex of the Göttingen minipig reveals patterns of spike activity at E110, which are highly similar to patterns recorded in prepubertal pig (Konda et al. 1979).

Referring to preterm human and newborn rats, electrophysiological recordings show that early visual responses to light stimuli are strongly amplified by the immature thalamocortical network (Colonnese et al. 2010). These network oscillations are presumed to prepare the VC for patterned vision. Shortly before birth in human and eye-opening in rat, a sudden switch to the mature visual response occurs. fMRI imaging reveals a quite dynamic landscape of transient functional connections between brain regions in early life (França et al. 2024). Moreover, spatiotemporal patterns of local cortical function and intrinsic coupling modes have been characterized in preterm infants as early as gestational week 33 (Yrjölä, Vanhatalo, and Tokariev 2024). Together, although the gestational stages are not always similar and difficult to align, these findings support the view that early neuronal activity, spontaneous and evoked by the periphery, is present before midgestation in ungulate and possibly in other mammals, too. The activity might trigger and promote vascular development if it remains at normal levels. Excessively high activity for instance by repetitive sensorimotor stimulation has a strong inhibitory effect on angiogenesis in the respective cortex area (Whiteus, Freitas, and Grutzendler 2014). Postnatally, activity-dependent remodeling can help to adapt the vasculature and thus the blood supply to the local demand.

Author Contributions

Conceptualization and methodology: E. S. and P. W. *Investigation and analysis*: E. S. and K. C. *Provided resources*: C. B., C. B., M. M., and D. U. *Visualization*: E. S., M. M., and D. U. *Writing—original draft*: E. S. and P. W. *writing—review and editing*: E. S., G. M., and P. W. *Supervision and project administration*: P. W. All authors approved the manuscript.

Acknowledgments

We acknowledge the Regionalverband Ruhr, Essen, Germany, for the interest in our work. We thank Andrea Räk and Christian Riedel for technical support. We thank Prof. Schmelz and Prof. Engelhardt, University Mannheim, Germany, for donating the P5 piglet brain.

Open access funding enabled and organized by Projekt DEAL.

Conflicts of Interest

The corresponding author, on behalf of the coauthors, declares no conflict of interest.

Ethics Statement

All applicable international, national, and/or institutional guidelines for the care and use of animals were followed. All procedures were in

accordance with the ethical standards or practice of the institution at which the studies were conducted.

Consent

The authors have nothing to report.

Data Availability Statement

All relevant data can be found within the article and its supplementary information and are openly available on bioRxiv (https://doi.org/10.1101/2024.05.17.594685).

Peer Review

The peer review history for this article is available at https://publons.com/publon/10.1002/cne.70011.

References

Allène, C., A. Cattani, J. B. Ackman, et al. 2008. "Sequential Generation of Two Distinct Synapse-Driven Network Patterns in Developing Neocortex." *Journal of Neuroscience* 28: 12851–12863. https://doi.org/10.1523/JNEUROSCI.3733-08.2008.

Alvarez-Vergara, M. I., A. E. Rosales-Nieves, R. March-Diaz, et al. 2021. "Non-Productive Angiogenesis Disassembles Aß Plaque-associated Blood Vessels." *Nature Communications* 12: 3098. https://doi.org/10.1038/s41467-021-23337-z.

Andreone, B. J., B. Lacoste, and C. Gu. 2015. "Neuronal and Vascular Interactions." *Annual Review of Neuroscience* 38: 25–46. https://doi.org/10.1146/annurev-neuro-071714-033835.

Armulik, A., G. Genové, M. Mäe, et al. 2010. "Pericytes Regulate the Blood-Brain Barrier." *Nature* 468: 557–561. https://doi.org/10.1038/nature09522.

Attwell, D., A. Mishra, C. N. Hall, F. M. O'Farrell, and T. Dalkara. 2016. "What Is a Pericyte?" *Journal of Cerebral Blood Flow and Metabolism* 36: 451–455. https://doi.org/10.1177/0271678x15610340.

Bandopadhyay, R., C. Orte, J. G. Lawrenson, A. R. Reid, S. S. De, and G. Allt. 2001. "Contractile Proteins in Pericytes at the Blood-Brain and Blood-Retinal Barriers." *Journal of Neurocytology* 30: 00–00. https://doi.org/10.1023/a:1011965307612.

Bass, N. H., H. H. Hess, A. Pope, and C. Thalheimer. 1971. "Quantitative Cytoarchitectonic Distribution of Neurons, Glia, and DNA in Rat Cerebral Cortex." *Journal of Comparative Neurology* 143: 481–490. https://doi.org/10.1002/cne.901430405.

Battistella, R., M. Kritsilis, H. Matuskova, et al. 2021. "Not all Lectins Are Equally Suitable for Labeling Rodent Vasculature." *International Journal of Molecular Sciences* 22: 00–00. https://doi.org/10.3390/ijms222111554.

Bell, M. A., and M. J. Ball. 1985. "Laminar Variation in the Microvascular Architecture of Normal human Visual Cortex (area 17)." *Brain Research* 335: 139–143. https://doi.org/10.1016/0006-8993(85)90284-7.

Benarroch, E. E. 2012. "Insulin-Like Growth Factors in the Brain and Their Potential Clinical Implications." *Neurology* 79: 2148–2153. https://doi.org/10.1212/WNL.0b013e3182752eef.

Biswas, S., A. Cottarelli, and D. Agalliu. 2020. "Neuronal and Glial Regulation of CNS Angiogenesis and Barriergenesis." *Development (Cambridge, England)* 147: 00–00. https://doi.org/10.1242/dev.182279.

Böndel, J. C. 2017. *Vergleichende morphometrische Untersuchungen am Gehirn von Sus scrofa und Sus scrofa f. domestica*, Ludwig-Maximilians-Universität München, Germany.

Boscia, F., C. L. Esposito, A. Casamassa, V. d. Franciscis, L. Annunziato, and L. Cerchia. 2013. "The Isolectin IB4 Binds RET Receptor Tyrosine Kinase in Microglia." *Journal of Neurochemistry* 126: 428–436. https://doi.org/10.1111/jnc.12209.

Bryant, A., Z. Li, R. Jayakumar, et al. 2023. "Endothelial Cells Are Heterogeneous in Different Brain Regions and Are Dramatically Altered in Alzheimer's Disease." *Journal of Neuroscience* 43: 4541–4557. https://doi.org/10.1523/JNEUROSCI.0237-23.2023.

Cassot, F., F. Lauwers, C. Fouard, S. Prohaska, and V. Lauwers-Cances. 2006. "A Novel Three-Dimensional Computer-Assisted Method for a Quantitative Study of Microvascular Networks of the Human Cerebral Cortex." *Microcirculation* 13: 1–18. https://doi.org/10.1080/10739680500383407.

Cayrol, R., K. Wosik, J. L. Berard, et al. 2008. "Activated Leukocyte Cell Adhesion Molecule Promotes Leukocyte Trafficking Into the central Nervous System." *Nature Immunology* 9: 137–145. https://doi.org/10.1038/ni1551.

Chand, K. K., S. M. Miller, G. J. Cowin, et al. 2022. "Neurovascular Unit Alterations in the Growth-restricted Newborn Are Improved Following ibuprofen Treatment." *Molecular Neurobiology* 59: 1018–1040. https://doi.org/10.1007/s12035-021-02654-w.

Clark, A. T., E. E. Abrahamson, M. M. Harper, and M. D. Ikonomovic. 2022. "Chronic Effects of Blast Injury on the Microvasculature in a Transgenic Mouse Model of Alzheimer's Disease Related Aβ Amyloidosis." *Fluids Barriers CNS* 19: 5. https://doi.org/10.1186/s12987-021-00301-z.

Colonnese, M. T., A. Kaminska, M. Minlebaev, et al. 2010. "A Conserved Switch in Sensory Processing Prepares Developing Neocortex for Vision." *Neuron* 67: 480–498. https://doi.org/10.1016/j.neuron.2010.07.015.

Cook, C. J., P. D. Gluckman, B. M. Johnston, and C. Williams. 1987. "The Development of the Somatosensory Evoked Potential in the Unanaesthetized Fetal Sheep." *Journal of Developmental Physiology* 9: 441–455.

Cragg, B. G. 1967. "The Density of Synapses and Neurones in the Motor and Visual Areas of the Cerebral Cortex." *Journal of Anatomy* 101: 639–654.

Crouch, E. E., A. Bhaduri, M. G. Andrews, et al. 2022. "Ensembles of Endothelial and Mural Cells Promote Angiogenesis in Prenatal human Brain." *Cell* 185: 3753–3769.e18. https://doi.org/10.1016/j.cell.2022.09.004.

Cucchi, T., D. Neaux, L. Féral, et al. 2024. "How Domestication, Feralization and Experience-dependent Plasticity Affect Brain Size Variation in *Sus scrofa*." *Royal Society Open Science* 11: 240951. https://doi.org/10.1098/rsos.240951.

Cummins, P. M. 2012. "Occludin: One Protein, Many Forms." *Molecular and Cellular Biology* 32: 242–250. https://doi.org/10.1128/MCB.06029-11.

Damisah, E. C., R. A. Hill, A. Rai, et al. 2020. "Astrocytes and Microglia Play Orchestrated Roles and Respect Phagocytic territories During Neuronal Corpse Removal in Vivo." *Science Advances* 6: eaba3239. https://doi.org/10.1126/sciadv.aba3239.

Daneman, R., L. Zhou, A. A. Kebede, and B. A. Barres. 2010. "Pericytes Are Required for Blood-brain Barrier Integrity During Embryogenesis." *Nature* 468: 562–566. https://doi.org/10.1038/nature09513.

Dziegielewska, K. M., C. A. Evans, D. H. Malinowska, et al. 1979. "Studies of the Development of Brain Barrier Systems to Lipid Insoluble Molecules in Fetal Sheep." *The Journal of Physiology* 292: 207–231.

Dziegielewska, K. M., L. A. Hinds, K. Møllgård, M. L. Reynolds, and N. R. Saunders. 1988. "Blood-brain, Blood-cerebrospinal Fluid and Cerebrospinal Fluid-brain Barriers in a Marsupial (Macropus eugenii) During Development." *The Journal of Physiology* 403: 367–388. https://doi.org/10.1113/jphysiol.1988.sp017254.

Ek, C. J., K. M. Dziegielewska, H. Stolp, and N. R. Saunders. 2006. "Functional Effectiveness of the Blood-brain Barrier to Small Water-soluble Molecules in Developing and Adult Opossum (Monodelphis domestica)." *Journal of Comparative Neurology* 496: 13–26. https://doi.org/10.1002/cne.20885.

Engelhardt, M., M. I. K. Hamad, A. Jack, et al. 2018. "Interneuron Synaptopathy in Developing Rat Cortex Induced by the Pro-Inflammatory

Cytokine LIF." *Experimental Neurology* 302: 169–180. https://doi.org/10.1016/j.expneurol.2017.12.011.

Ernst, L., S. Darschnik, J. Roos, et al. 2018. "Fast Prenatal Development of the NPY Neuron System in the Neocortex of the European Wild Boar, Sus scrofa." *Brain Struct Funct* 223: 3855–3873. https://doi.org/10.1007/s00429-018-1725-y.

Feeney, J. F., and R. L. Watterson. 1946. "The Development of the Vascular Pattern Within the Walls of the central Nervous System of the Chick Embryo." *Journal of Morphology* 78: 231–303. https://doi.org/10.1002/jmor.1050780205.

Fonta, C., and M. Imbert. 2002. "Vascularization in the Primate Visual Cortex During Development." *Cerebral Cortex* 12: 199–211. https://doi.org/10.1093/cercor/12.2.199.

França, L. G. S., J. Ciarrusta, O. Gale-Grant, et al. 2024. "Neonatal Brain Dynamic Functional Connectivity in Term and Preterm Infants and Its Association With Early Childhood Neurodevelopment." *Nature Communications* 15: 16. https://doi.org/10.1038/s41467-023-44050-z.

Gama Sosa, M. A., R. d. Gasperi, G. M. Perez, P. R. Hof, and G. A. Elder. 2021. "Hemovasculogenic Origin of Blood Vessels in the Developing Mouse Brain." *Journal of Comparative Neurology* 529: 340–366. https://doi.org/10.1002/cne.24951.

Gittins, R., and P. J. Harrison. 2004. "Neuronal Density, Size and Shape in the human Anterior Cingulate Cortex: a Comparison of Nissl and NeuN Staining." *Brain Research Bulletin* 63: 155–160. https://doi.org/10.1016/j.brainresbull.2004.02.005.

Gredal, O., H. Pakkenberg, M. Karlsborg, and B. Pakkenberg. 2000. "Unchanged Total Number of Neurons in Motor Cortex and Neocortex in Amyotrophic Lateral Sclerosis: a Stereological Study." *Journal of Neuroscience Methods* 95: 171–176. https://doi.org/10.1016/S0165-0270(99)00175-2.

Greene, C., J. Kealy, M. M. Humphries, et al. 2017. "Dose-dependent Expression of Claudin-5 Is a Modifying Factor in Schizophrenia." *Molecular Psychiatry* 23: 2156–2166. https://doi.org/10.1038/mp.2017.156.

Grubb, S., C. Cai, B. O. Hald, et al. 2020. "Precapillary Sphincters Maintain Perfusion in the Cerebral Cortex." *Nature Communications* 11: 395. https://doi.org/10.1038/s41467-020-14330-z.

Hagemann, N., Y. Qi, A. Mohamud Yusuf, et al. 2024. "Microvascular Network Remodeling in the Ischemic Mouse Brain Defined by Light Sheet Microscopy." *Arteriosclerosis, Thrombosis, and Vascular Biology* 44: 915–929. https://doi.org/10.1161/ATVBAHA.123.320339.

Hahn, A., J. Bode, A. Alexander, et al. 2021. "Large-scale Characterization of the Microvascular Geometry in Development and Disease by Tissue Clearing and Quantitative Ultramicroscopy." *Journal of Cerebral Blood Flow and Metabolism* 41: 1536–1546. https://doi.org/10.1177/0271678x20961854.

Hall, C. N., C. Reynell, B. Gesslein, et al. 2014. "Capillary Pericytes Regulate Cerebral Blood Flow in Health and Disease." *Nature* 508: 55–60. https://doi.org/10.1038/nature13165.

Harris, A. P., H. Ohata, and R. C. Koehler. 2008. "Role of Nitric Oxide in Cerebrovascular Reactivity to NMDA and Hypercapnia During Prenatal Development in Sheep." *International Journal of Developmental Neuroscience* 26: 47–55. https://doi.org/10.1016/j.ijdevneu.2007.08.011.

Haruwaka, K., A. Ikegami, Y. Tachibana, et al. 2019. "Dual Microglia Effects on Blood Brain Barrier Permeability Induced by Systemic Inflammation." *Nature Communications* 10: 5816. https://doi.org/10.1038/s41467-019-13812-z.

Haug, H. 1971. "Die Membrana Limitans Gliae Superficialis Der Sehrinde Der Katze." *Z Zellforsch* 115: 79–87. https://doi.org/10.1007/BF00330216.

Heinzer, S., T. Krucker, M. Stampanoni, et al. 2006. "Hierarchical Microimaging for Multiscale Analysis of Large Vascular Networks." *Neuroimage* 32: 626–636. https://doi.org/10.1016/j.neuroimage.2006.03.043.

Hellström, M., H. Gerhardt, M. Kalén, et al. 2001. "Lack of Pericytes Leads to Endothelial Hyperplasia and Abnormal Vascular Morphogenesis." *Journal of Cell Biology* 153: 543–553. https://doi.org/10.1083/jcb.153.3.543.

Henry, V. G. 1968. "Fetal Development in European Wild Hogs." *The Journal of Wildlife Management* 32: 966. https://doi.org/10.2307/3799577.

Herculano-Houzel, S., B. Mota, and R. Lent. 2006. "Cellular Scaling Rules for Rodent Brains." *PNAS* 103: 12138–12143. https://doi.org/10.1073/pnas.0604911103.

Hoeffel, G., and F. Ginhoux. 2018. "Fetal Monocytes and the Origins of Tissue-Resident Macrophages." *Cellular Immunology* 330: 5–15. https://doi.org/10.1016/j.cellimm.2018.01.001.

Hsu, C.-W., J. Cerda, J. M. Kirk, et al. 2022. "EZ Clear for Simple, Rapid, and Robust Mouse Whole Organ Clearing." *Elife* 11: 00–00. https://doi.org/10.7554/eLife.77419.

Irintchev, A., A. Rollenhagen, E. Troncoso, J. Z. Kiss, and M. Schachner. 2005. "Structural and Functional Aberrations in the Cerebral Cortex of Tenascin-C Deficient Mice." *Cerebral Cortex* 15: 950–962. https://doi.org/10.1093/cercor/bhh195.

Ishihara, K., K. Takata, and K.-I. Mizutani. 2023. "Involvement of an Aberrant Vascular System in Neurodevelopmental, Neuropsychiatric, and Neuro-degenerative Diseases." *Life* 13: 00–00. https://doi.org/10.3390/life13010221.

Ji, X., T. Ferreira, B. Friedman, et al. 2021. "Brain Microvasculature Has a Common Topology With Local Differences in Geometry That Match Metabolic Load." *Neuron* 109: 1168–1187.e13. https://doi.org/10.1016/j.neuron.2021.02.006.

Kaushik, D. K., A. Bhattacharya, B. M. Lozinski, and V. Wee Yong. 2021. "Pericytes as Mediators of Infiltration of Macrophages in Multiple Sclerosis." *J Neuroinflammation* 18: 301. https://doi.org/10.1186/s12974-021-02358-x.

Kaushik, G., K. Gupta, V. Harms, et al. 2020. "Engineered Perineural Vascular Plexus for Modeling Developmental Toxicity." *Adv Healthc Mater* 9: e2000825. https://doi.org/10.1002/adhm.202000825.

Kisler, K., A. R. Nelson, A. Montagne, and B. V. Zlokovic. 2017a. "Cerebral Blood Flow Regulation and Neurovascular Dysfunction in Alzheimer disease." *Nature Reviews Neuroscience* 18: 419–434. https://doi.org/10.1038/nrn.2017.48.

Kisler, K., A. R. Nelson, S. V. Rege, et al. 2017b. "Pericyte Degeneration Leads to Neurovascular Uncoupling and Limits Oxygen Supply to Brain." *Nature Neuroscience* 20: 406–416. https://doi.org/10.1038/nn.4489.

Komabayashi-Suzuki, M., E. Yamanishi, C. Watanabe, et al. 2019. "Spatiotemporally Dependent Vascularization Is Differently Utilized Among Neural Progenitor Subtypes During Neocortical Development." *Cell reports* 29: 1113–1129.e5. https://doi.org/10.1016/j.celrep.2019.09.048.

Konda, N., R. G. Dyer, T. Bruhn, A. A. Macdonald, and F. Ellendorff. 1979. "A Method for Recording Single Unit Activity From the Brains of Foetal Pigs in Utero." *Journal of Neuroscience Methods* 1: 289–300. https://doi.org/10.1016/0165-0270(79)90040-2.

Kozma, M., Á. Mészáros, Á. Nyúl-Tóth, et al. 2021. "Cerebral Pericytes and Endothelial Cells Communicate Through Inflammasome-dependent Signals." *International Journal of Molecular Sciences* 22: 00–00. https://doi.org/10.3390/ijms22116122.

Kurz, H., T. Gärtner, P. S. Eggli, and B. Christ. 1996. "First Blood Vessels in the avian Neural Tube Are Formed by a Combination of Dorsal Angioblast Immigration and Ventral Sprouting of Endothelial Cells." *Developmental Biology* 173: 133–147. https://doi.org/10.1006/dbio.1996.0012.

Lauwers, F., F. Cassot, V. Lauwers-Cances, P. Puwanarajah, and H. Duvernoy. 2008. "Morphometry of the human Cerebral Cortex Microcirculation: General Characteristics and Space-related Profiles." *Neuroimage* 39: 936–948. https://doi.org/10.1016/j.neuroimage.2007.09.024.

Lidow, M. S., P. S. Goldman-Rakic, and P. Rakic. 1991. "Synchronized Overproduction of Neurotransmitter Receptors in Diverse Regions of the

Primate Cerebral Cortex." *PNAS* 88: 10218–10221. https://doi.org/10.1073/pnas.88.22.10218.

Linné, C. v. 1758. *Systema naturae per regna tria naturae:secundum classes, ordines, genera, species, cum characteribus, differentiis, synonymis, locis*. Stockholm, Sweden: Impensis Direct. Laurentii Salvii.

Liu, L.-R., J.-C. Liu, J.-S. Bao, Q.-Q. Bai, and G.-Q. Wang. 2020. "Interaction of Microglia and Astrocytes in the Neurovascular Unit." *Frontiers in immunology* 11: 1024. https://doi.org/10.3389/fimmu.2020.01024.

Luhmann, H. J., A. Sinning, J.-W. Yang, et al. 2016. "Spontaneous Neuronal Activity in Developing Neocortical Networks: from Single Cells to Large-scale Interactions." *Front Neural Circuits* 10: 40. https://doi.org/10.3389/fncir.2016.00040.

Mäe, M. A., L. He, S. Nordling, et al. 2021. "Single-cell Analysis of Blood-brain Barrier Response to Pericyte Loss." *Circulation Research* 128: e46–e62. https://doi.org/10.1161/CIRCRESAHA.120.317473.

Mathiisen, T. M., K. P. Lehre, N. C. Danbolt, and O. P. Ottersen. 2010. "The Perivascular Astroglial Sheath Provides a Complete Covering of the Brain Microvessels: an Electron Microscopic 3D Reconstruction." *Glia* 58: 1094–1103. https://doi.org/10.1002/glia.20990.

Meyer, G. 2010. "Building a human Cortex: the Evolutionary Differentiation of Cajal-Retzius Cells and the Cortical Hem." *Journal of Anatomy* 217: 334–343. https://doi.org/10.1111/j.1469-7580.2010.01266.x.

Michaloudi, H., I. Grivas, C. Batzios, M. Chiotelli, and G. C. Papadopoulos. 2005. "Areal and Laminar Variations in the Vascularity of the Visual, Auditory, and Entorhinal Cortices of the Developing Rat Brain." *Developmental Brain Research* 155: 60–70. https://doi.org/10.1016/j.devbrainres.2004.11.007.

Møllgård, K., F. R. M. Beinlich, P. Kusk, et al. 2023. "A Mesothelium Divides the Subarachnoid Space Into Functional Compartments." *Science* 379: 84–88. https://doi.org/10.1126/science.adc8810.

Mollgøard, K., and N. R. Saunders. 1975. "Complex Tight Junctions of Epithelial and of Endothelial Cells in Early Foetal Brain." *Journal of Neurocytology* 4: 453–468. https://doi.org/10.1007/BF01261375.

Molliver, M. E. 1967. "An Ontogenetic Study of Evoked Somesthetic Cortical Responses in the Sheep." *Progress in Brain Research* 26: 78–91. https://doi.org/10.1016/S0079-6123(08)61420-X.

Olsson, Y., I. Klatzo, P. Sourander, and O. Steinwall. 1968. "Blood-Brain Barrier to Albumin in Embryonic New Born and Adult Rats." *Acta Neuropathologica* 10: 117–122. https://doi.org/10.1007/BF00691305.

Ouellette, J., and B. Lacoste. 2021. "From Neurodevelopmental to Neurodegenerative Disorders: The Vascular Continuum." *Frontiers in aging neuroscience* 13: 00–00. https://doi.org/10.3389/fnagi.2021.749026.

Pandey, K., B. Bessières, S. L. Sheng, et al. 2023. "Neuronal Activity Drives IGF2 Expression From Pericytes to Form Long-term Memory." *Neuron*. https://doi.org/10.1016/j.neuron.2023.08.030.

Penna, E., J. M. Mangum, H. Shepherd, V. Martínez-Cerdeño, and S. C. Noctor. 2021. "Development of the Neuro-Immune-Vascular Plexus in the Ventricular Zone of the Prenatal Rat Neocortex." *Cerebral Cortex* 31: 2139–2155. https://doi.org/10.1093/cercor/bhaa351.

Persson, H. E., and D. Stenberg. 1972. "Early Prenatal Development of Cortical Surface Responses to Visual Stimuli in Sheep." *Experimental Neurology* 37: 199–208. https://doi.org/10.1016/0014-4886(72)90236-1.

Powell, N. J., B. Hein, D. Kong, et al. 2024. "Common Modular Architecture Across Diverse Cortical Areas in Early Development." *PNAS* 121: e2313743121. https://doi.org/10.1073/pnas.2313743121.

Reynolds, M. L., M. E. Cavanagh, K. M. Dziegielewska, L. A. Hinds, N. R. Saunders, and C. H. Tyndale-Biscoe. 1985. "Postnatal Development of the Telencephalon of the tammar Wallaby (Macropus eugenii). An accessible model of neocortical differentiation." *Anat Embryol* 173: 81–94. https://doi.org/10.1007/BF00707306.

Risau, W., R. Hallmann, and U. Albrecht. 1986. "Differentiation-Dependent Expression of Proteins in Brain Endothelium During Development of the Blood-brain Barrier." *Developmental Biology* 117: 537–545. https://doi.org/10.1016/0012-1606(86)90321-0.

Risser, L., F. Plouraboué, P. Cloetens, and C. Fonta. 2009. "A 3D-Investigation Shows That Angiogenesis in Primate Cerebral Cortex Mainly Occurs at Capillary Level." *International Journal of Developmental Neuroscience* 27: 185–196. https://doi.org/10.1016/j.ijdevneu.2008.10.006.

Ritter, C., L. Eigen, N. Deiringer, L. Laubscher, and M. Brecht. 2023. "Coevolution of Rostrum and Brain in Pig Species." *Journal of Comparative Neurology* 531: 775–789. https://doi.org/10.1002/cne.25461.

Roessmann, U., and P. Gambetti. 1986. "Astrocytes in the Developing human Brain. An Immunohistochemical Study." *Acta Neuropathologica* 70: 308–313. https://doi.org/10.1007/BF00686089.

Sadowska, G. B., N. Ahmedli, X. Chen, and B. S. Stonestreet. 2015. "Ontogeny of Tight Junction Protein Expression in the Ovine Cerebral Cortex During Development." *Neuroscience* 310: 422–429. https://doi.org/10.1016/j.neuroscience.2015.09.062.

Segarra, M., M. R. Aburto, J. Hefendehl, and A. Acker-Palmer. 2019. "Neurovascular Interactions in the Nervous System." *Annual Review of Cell and Developmental Biology* 35: 615–635. https://doi.org/10.1146/annurev-cellbio-100818-125142.

Shapson-Coe, A., M. Januszewski, D. R. Berger, et al. 2024. "A Petavoxel Fragment of human Cerebral Cortex Reconstructed at Nanoscale Resolution." *Science* 384: eadk4858. https://doi.org/10.1126/science.adk4858.

Smyth, L. C. D., J. Rustenhoven, E. L. Scotter, et al. 2018. "Markers for human Brain Pericytes and Smooth Muscle Cells." *Journal of Chemical Neuroanatomy* 92: 48–60. https://doi.org/10.1016/j.jchemneu.2018.06.001.

Smyth, L. C. D., D.i Xu, S. V. Okar, et al. 2024. "Identification of Direct Connections Between the Dura and the Brain." *Nature* 627: 00–00. https://doi.org/10.1038/s41586-023-06993-7.

Sobierajski, E., G. Lauer, M. Aktas, et al. 2022. "Development of Microglia in Fetal and Postnatal Neocortex of the Pig, the European Wild Boar (Sus scrofa)." *Journal of Comparative Neurology* 530: 1341–1362. https://doi.org/10.1002/cne.25280.

Sobierajski, E., G. Lauer, K. Czubay, et al. 2023. "Development of Myelin in Fetal and Postnatal Neocortex of the Pig, the European Wild Boar Sus scrofa." *Brain Struct Funct* 228: 947–966. https://doi.org/10.1007/s00429-023-02633-y.

Stewart, P. A., and E. M. Hayakawa. 1987. "Interendothelial Junctional Changes Underlie the Developmental 'Tightening' of the Blood-Brain Barrier." *Brain Research* 429: 271–281. https://doi.org/10.1016/0165-3806(87)90107-6.

Stewart, P. A., and M. J. Wiley. 1981. "Developing Nervous Tissue Induces Formation of Blood-brain Barrier Characteristics in Invading Endothelial Cells: a Study Using Quail—Chick Transplantation Chimeras." *Developmental Biology* 84: 183–192. https://doi.org/10.1016/0012-1606(81)90382-1.

Take, Y., Y. Chikai, K. Shimamori, M. Kuragano, H. Kurita, and K. Tokuraku. 2022. "Amyloid β Aggregation Induces human Brain Microvascular Endothelial Cell Death With Abnormal Actin Organization." *Biochem Biophys Rep* 29: 101189. https://doi.org/10.1016/j.bbrep.2021.101189.

Tan, X., W. A. Liu, X.-J. Zhang, et al. 2016. "Vascular Influence on Ventral Telencephalic Progenitors and Neocortical Interneuron Production." *Developmental Cell* 36: 624–638. https://doi.org/10.1016/j.devcel.2016.02.023.

Teng, J., Y. Gao, H. Yin, et al. 2024. "A Compendium of Genetic Regulatory Effects Across Pig Tissues." *Nature Genetics* 56: 112–123. https://doi.org/10.1038/s41588-023-01585-7.

Thomas, J.-L. 2018. "Orchestrating Cortical Brain Development." *Science* 361: 754–755. https://doi.org/10.1126/science.aau7155.

Thurgur, H., and E. Pinteaux. 2019. "Microglia in the Neurovascular Unit: Blood-Brain Barrier-microglia Interactions After central Nervous

System Disorders." *Neuroscience* 405: 55–67. https://doi.org/10.1016/j.neuroscience.2018.06.046.

Tieman, S. B., S. Möllers, D. G. Tieman, and J. White. 2004. "The Blood Supply of the Cat's Visual Cortex and Its Postnatal Development." *Brain Research* 998: 100–112. https://doi.org/10.1016/j.brainres.2003.11.023.

Tsai, P. S., J. P. Kaufhold, P. Blinder, et al. 2009. "Correlations of Neuronal and Microvascular Densities in Murine Cortex Revealed by Direct Counting and Colocalization of Nuclei and Vessels." *Journal of Neuroscience* 29: 14553–14570. https://doi.org/10.1523/JNEUROSCI.3287-09.2009.

Veersema, T. J., A. d. Neef, J. van Scheppingen, et al. 2019. "Changes in Vascular Density in Resected Tissue of 97 Patients With Mild Malformation of Cortical Development, Focal Cortical Dysplasia or TSC-Related Cortical Tubers." *International Journal of Developmental Neuroscience* 79: 96–104. https://doi.org/10.1016/j.ijdevneu.2019.11.003.

Virgintino, D., D. Robertson, V. Benagiano, et al. 2000. "Immunogold Cytochemistry of the Blood-Brain Barrier Glucose Transporter GLUT1 and Endogenous Albumin in the Developing human Brain." *Developmental Brain Research* 123: 95–101. https://doi.org/10.1016/S0165-3806(00)00086-9.

Wahle, P., E. Sobierajski, I. Gasterstädt, et al. 2022. "Neocortical Pyramidal Neurons With Axons Emerging From Dendrites are Frequent in Non-Primates, but Rare in Monkey and Human." *Elife* 11: e76101. http://doi.org/10.7554/eLife.76101.

Weber, B., A. L. Keller, J. Reichold, and N. K. Logothetis. 2008. "The Microvascular System of the Striate and Extrastriate Visual Cortex of the Macaque." *Cerebral Cortex* 18: 2318–2330. https://doi.org/10.1093/cercor/bhm259.

Whiteus, C., C. Freitas, and J. Grutzendler. 2014. "Perturbed Neural Activity Disrupts Cerebral Angiogenesis During a Postnatal Critical Period." *Nature* 505: 407–411. https://doi.org/10.1038/nature12821.

Woods, J. R., and M. A. Plessinger. 1986. "The Fetal Visual Evoked Potential." *Pediatric Research* 20: 351–355. https://doi.org/10.1203/00006450-198604000-00019.

Wu, C. H., C. Y. Wen, J. Y. Shieh, and E. A. Ling. 1994. "Down-regulation of Membrane Glycoprotein in Amoeboid Microglia Transforming Into Ramified Microglia in Postnatal Rat Brain." *Journal of Neurocytology* 23: 258–269. https://doi.org/10.1007/BF01275530.

Wu, J. Y., S.-J. Cho, K. Descant, et al. 2024. "Mapping of Neuronal and Glial Primary Cilia Contactome and Connectome in the human Cerebral Cortex." *Neuron* 112: 41–55.e3. https://doi.org/10.1016/j.neuron.2023.09.032.

Wu, J., Y. He, Z. Yang, et al. 2014. "3D BrainCV: Simultaneous Visualization and Analysis of Cells and Capillaries in a Whole Mouse Brain With One-micron Voxel Resolution." *Neuroimage* 87: 199–208. https://doi.org/10.1016/j.neuroimage.2013.10.036.

Yrjölä, P., S. Vanhatalo, and A. Tokariev. 2024. "Neuronal Coupling Modes Show Differential Development in the Early Cortical Activity Networks of human Newborns." *Journal of Neuroscience* 44: 00–00. https://doi.org/10.1523/JNEUROSCI.1012-23.2024.

Zilles, K., N. Palomero-Gallagher, and K. Amunts. 2013. "Development of Cortical Folding During Evolution and Ontogeny." *Trends in Neuroscience (Tins)* 36: 275–284. https://doi.org/10.1016/j.tins.2013.01.006.